Joint Communication and Localization in Millimeter Wave Networks

Girim Kwon, *Member, IEEE*, Andrea Conti, *Senior Member, IEEE*, Hyuncheol Park, *Senior Member, IEEE*, and Moe Z. Win, *Fellow, IEEE*

Abstract—**Joint communication and localization will be a key in beyond 5G networks for emerging context-aware applications such as Internet-of-Things and autonomous vehicles. In particular, millimeter wave (mmWave) networks using a massive number of antennas and large bandwidth are considered for high-rate communication and high-accuracy localization. In mmWave networks, beamforming (BF) and power allocation need to be jointly designed to simultaneously achieve high data rates and high localization accuracies. This paper proposes cooperative BF and power allocation scheme with multiple base stations to maximize the weighted sum rate of mobile stations while guaranteeing position and orientation estimation error bounds. The proposed scheme consists of two stages. In the first stage, pilot overhead is minimized while satisfying the accuracy constraints. In the second stage, the weighted sum rate for data transmission is maximized based on the estimated channel information. Numerical results show that the proposed scheme achieves a larger rate-accuracy region compared to conventional schemes.**

Index Terms—**Joint communication and localization, millimeter wave, user-centric network, beamforming, power allocation.**

I. INTRODUCTION

JOINT communication and localization is expected to be one of the key drivers for beyond 5G wireless applications relying on position information [1]–[3] including autonomy [4]–[6], crowd sensing [7]–[9], smart

Fig. 1. Joint communication and localization systems with N_{BS} BSs and N_{MS} MSs in mmWave downlink channels.

Girim Kwon is with the Wireless Information and Network Sciences Laboratory, Massachusetts Institute of Technology, Cambridge, MA 02139 USA (e-mail: girimk@mit.edu).

Andrea Conti is with the Department of Engineering and CNIT, University of Ferrara, 44122 Ferrara, Italy (e-mail: a.conti@ieee.org).

Hyuncheol Park is with the School of Electrical Engineering, Korea Advanced Institute of Science and Technology, Daejeon 34141, Republic of Korea (e-mail: hcpark@kaist.ac.kr).

Moe Z. Win is with the Laboratory for Information and Decision Systems, Massachusetts Institute of Technology, Cambridge, MA 02139 USA (e-mail: moewin@mit.edu).

environments [10]–[12], assets tracking [13]–[15], and the Internet-of-Things (IoT) [16]–[18]. The quality of experience in wireless networks highly depends on both the accuracy of location awareness and the communication capability. The simultaneous provision of communication and localization functionalities is challenged by the fact that they share a limited amount of wireless resources, such as frequency, time, and power. For example, when communication and localization signals are orthogonally transmitted in different time-frequency resources, an increase in the data rate for communication would result in a degradation of localization accuracy and vice versa.

Location awareness can be achieved for both network nodes and unconnected objects, respectively referred to as active [19]–[32] and passive localization [33]–[53]. Active localization [19]–[32] has attracted interest in millimeter wave (mmWave) multiple-input multiple-output (MIMO) systems as accurate estimates of distances and angles are possible by exploiting antenna arrays and large bandwidth (see Fig. 1). Passive localization has been extensively studied for coexistence of radar and communication networks [33]–[39], dual-functional radar-communication systems [39]–[50], and perceptive mobile networks [51]–[53].

MIMO systems have been extensively investigated in the past [54]–[66]. In the context of location-aware beamforming (BF), the trade-off between data rate and localization accuracy

needs careful attention [67]–[69]. In [67], the BF scheme was designed to minimize the transmitted power, while satisfying the rate and positioning error requirements. In [68], the rate maximization problem and the squared positioning error minimization problem were solved for MIMO systems with finite-resolution front-ends. In [69], the effect of power optimization on the rate-accuracy trade-off was investigated assuming perfect channel state information (CSI). The works in [67]–[69] have assumed that localization is performed during data transmission after pilot transmission. However, localization can also be performed together with channel estimation during the pilot transmission period. In this case, the duration of pilot and data transmission periods can be optimized for a given channel coherence time. In addition, analog-digital hybrid BF structure can be considered for efficient implementation of mmWave MIMO systems [70]–[73].

In mmWave networks, it is crucial to develop cooperative BF techniques for user-centric networks where a mobile station (MS) can receive the desired signals from multiple neighboring base stations (BSs). User-centric networks can overcome the link blockage in mmWave channel and the cell-edge problems in conventional cellular network [74]–[76].

The fundamental questions related to joint communication and localization in mmWave networks are the following.
- How to balance the channel utilization of pilot and data signals within a limited time?
- How to allocate data rate and localization accuracy for users in different locations?

The answers to these questions will accelerate the realization of the aforementioned applications in beyond 5G wireless networks. Accordingly, we aim to enlarge the rate-accuracy region of the joint communication and localization system. The main challenge is to jointly design the pilot sequence, BF, and power allocation of multiple BSs and MSs. In particular, it is important to account for channel estimation error and analog-digital hybrid BF structure in realistic mmWave systems.

This paper develops mmWave networks for joint communication and localization, accounting for channel estimation errors and analog-digital hybrid BF structures. The key contributions of this paper are as follows:
- solving the weighted sum rate maximization problem under accuracy constraints with analog-digital hybrid BF;
- deriving the asymptotic rate expression for MIMO systems with imperfect channel estimation; and
- quantifying the gain of the proposed scheme over benchmark schemes in terms of the rate-accuracy region.

The remaining sections are organized as follows: Section II describes the system model. Section III introduces the performance metrics. Section IV presents the proposed scheme. Section V shows the simulation results. Finally, Section VI gives our conclusions.

Notations: Random variables are displayed in sans serif, upright fonts; their realizations in serif, italic fonts. Vectors and matrices are denoted by bold lowercase and uppercase letters, respectively. For example, a random variable and its realization are denoted by X and x for scalars, $\mathbf{x}$ and $\boldsymbol{x}$ for vectors, and $\mathbf{X}$ and $\boldsymbol{X}$ for matrices. A random set and its realization are denoted

by X and $\mathcal{X}$, respectively. The m-dimensional vector of ones is denoted by $\mathbf{1}_m$. The m-by-m identity matrix is denoted by $\boldsymbol{I}_m$. The ith element of $\boldsymbol{x}$ is denoted by $[\boldsymbol{x}]_i$, and the ith row and jth column of $\boldsymbol{X}$ is denoted by $[\boldsymbol{X}]_{i,j}$, where an index can be substituted by a range, i.e. $a{:}b$, representing a set of consecutive indices from a to b. The transpose, conjugate, and conjugate transpose are denoted by $(\cdot)^{\mathrm{T}}$, $(\cdot)^*$, and $(\cdot)^{\dagger}$, respectively. The matrix inequality $\boldsymbol{X} \succeq \boldsymbol{Y}$ means that $\boldsymbol{X} - \boldsymbol{Y}$ is positive semidefinite. The real and imaginary parts of a complex number are denoted by $\Re\{\cdot\}$ and $\Im\{\cdot\}$, respectively. The expectation is denoted by $\mathbb{E}\{\cdot\}$. The generalized delta function $\delta(x)$ is defined as $\delta(x) = 1$ for $x = 0$ and $\delta(x) = 0$ for $x \neq 0$. The estimated version of X is denoted by $\widehat{\mathsf{X}}$.

II. SYSTEM MODEL

This section describes the system operation for joint communication and localization. The mathematical representations for mmWave channel and received signals are also presented here, which are used for defining performance metrics and developing algorithms in the next sections.

A. Joint Communication and Localization in User-Centric mmWave Networks

Consider a joint communication and localization network with N_{BS} BSs each with N_{tx} transmitting antennas at known positions, denoted by $\boldsymbol{q}_1, \boldsymbol{q}_2, \ldots, \boldsymbol{q}_{N_{\mathrm{BS}}}$ with known orientation angles of $(\phi_n^{\mathrm{t}}, \theta_n^{\mathrm{t}})$ for $n = 1, 2, \ldots, N_{\mathrm{BS}}$. The network consists also of N_{MS} MSs each with N_{rx} receiving antennas at unknown positions, denoted by $\boldsymbol{p}_1, \boldsymbol{p}_2, \ldots, \boldsymbol{p}_{N_{\mathrm{MS}}}$ with unknown orientation angles of $(\phi_k^{\mathrm{r}}, \theta_k^{\mathrm{r}})$ for $k = 1, 2, \ldots, N_{\mathrm{MS}}$. As illustrated in Fig. 1, the BSs cooperatively transmit the signals to the MSs in mmWave downlink channels. Within a channel coherence time T_{c} the pilot symbols and data symbols are transmitted, respectively over periods T_{p} and T_{d}, with $T_{\mathrm{c}} = T_{\mathrm{p}} + T_{\mathrm{d}}$. The time periods are also expressed with the unit of symbol period T_{s} such that $T_{\mathrm{c}} = N_{\mathrm{p}}T_{\mathrm{s}} + N_{\mathrm{d}}T_{\mathrm{s}}$, where N_{p} and N_{d} are the numbers of transmitted symbols for pilot and data transmissions, respectively. Specifically, the system operates as follows. Using the positional information from global navigation satellite system (GNSS) of each MS, the BSs determine the BF matrices for pilot transmissions. The channels, positions, and orientations of the MSs are estimated during pilot transmission period, T_{p}. Using the estimated information of the channel parameters and localization parameters, BF and power allocation are determined for data transmission. Finally, data streams are transmitted during data transmission period, T_{d}.

The transmit BF matrices at the nth BS are denoted by $\mathbf{F}_n^{\mathrm{p}} \in \mathbb{C}^{N_{\mathrm{tx}} \times N_{\mathrm{MS}}}$ and $\mathbf{F}_n^{\mathrm{d}} \in \mathbb{C}^{N_{\mathrm{tx}} \times N_{\mathrm{MS}}}$ for pilot transmission and data transmission, respectively. To reduce the hardware complexity and power consumption of the mmWave BF system, we adopt the hybrid BF structure such that $\mathbf{F}_n^{\mathrm{p}} = \hat{\mathbf{F}}_n^{\mathrm{p}}\breve{\mathbf{F}}_n^{\mathrm{p}}$ and $\mathbf{F}_n^{\mathrm{d}} = \hat{\mathbf{F}}_n^{\mathrm{d}}\breve{\mathbf{F}}_n^{\mathrm{d}}$. The radiofrequency (RF) BF matrices consisting of RF phase shifters are denoted by $\hat{\mathbf{F}}_n^{\mathrm{p}} \in \mathbb{C}^{N_{\mathrm{tx}} \times \hat{N}_{\mathrm{tx}}}$ and $\hat{\mathbf{F}}_n^{\mathrm{d}} \in \mathbb{C}^{N_{\mathrm{tx}} \times \hat{N}_{\mathrm{tx}}}$, which cannot control the magnitude of the signals, where $\hat{N}_{\mathrm{tx}}$ is the number of RF chains at the BS. The baseband BF matrices

are denoted by $\check{\mathbf{F}}_n^{\mathrm{p}}$ and $\check{\mathbf{F}}_n^{\mathrm{d}}$. For pilot transmission, we assume that inaccurate location information of the MSs are available at the BSs via GNSS, which are then used for designing $\mathbf{F}_n^{\mathrm{p}}$. For data transmission, the matrix $\mathbf{F}_n^{\mathrm{d}}$ depends on the estimated angle-of-departure (AoD), which are fed back from the MSs. Meanwhile, the receive BF vector at the kth MS is only used in data transmission period by exploiting the estimated CSI. This vector is denoted by $\mathbf{w}_k^{\mathrm{d}} = \hat{\mathbf{W}}_k^{\mathrm{d}} \check{\mathbf{w}}_k^{\mathrm{d}}$ where $\hat{\mathbf{W}}_k^{\mathrm{d}} \in \mathbb{C}^{N_{\mathrm{rx}} \times \hat{N}_{\mathrm{rx}}}$ is the RF BF matrix, and $\check{\mathbf{w}}_k^{\mathrm{d}}$ is the baseband BF vector. For simplicity, we assume $\hat{N}_{\mathrm{tx}} = N_{\mathrm{MS}}$ and $\hat{N}_{\mathrm{rx}} = N_{\mathrm{BS}}$ in our system.

B. Channel Model

The mmWave channel between the nth BS and the kth MS at time t is expressed by an $N_{\mathrm{rx}} \times N_{\mathrm{tx}}$ matrix as [77]

$$\tilde{\mathbf{H}}_{n,k}(t) = \sum_{l=1}^{L} \mathbf{H}_{n,k,l}\, \delta(t - \tau_{n,k,l}) \tag{1}$$

with

$$\mathbf{H}_{n,k,l} = \sqrt{N_{\mathrm{tx}} N_{\mathrm{rx}}}\, \alpha_{n,k,l}\, \boldsymbol{a}_{\mathrm{r}}(\varphi_{n,k,l}^{\mathrm{r}}, \theta_{n,k,l}^{\mathrm{r}})\, \boldsymbol{a}_{\mathrm{t}}^{\dagger}(\varphi_{n,k,l}^{\mathrm{t}}, \theta_{n,k,l}^{\mathrm{t}}).$$

In (1), $\tau_{n,k,l}$ is the time delay of the lth path between the nth BS and the kth MS; $\alpha_{n,k,l}$ is the corresponding random complex gain distributed as $\mathcal{CN}(0, (\bar{H}_{n,k}^{(\mathrm{L})})^2)$ if $l = 1$ and $\mathcal{CN}(0, (\bar{H}_{n,k}^{(\mathrm{N})})^2)$ if $l > 1$, where $\bar{H}_{n,k}^{(\mathrm{L})}$ and $\bar{H}_{n,k}^{(\mathrm{N})}$ represent the large-scale channel gains for line-of-sight (LOS) and non-line-of-sight (NLOS) components, respectively; $\boldsymbol{a}_{\mathrm{r}}(\cdot)$ represents array response vector of the MSs; $\boldsymbol{a}_{\mathrm{t}}(\cdot)$ represents array steering vector of the BSs; $\varphi_{n,k,l}^{\mathrm{r}}$ and $\theta_{n,k,l}^{\mathrm{r}}$ are azimuth and zenith angle-of-arrivals (AoAs) of the lth path between the nth BS and the kth MS, respectively; Similarly, $\varphi_{n,k,l}^{\mathrm{t}}$ and $\theta_{n,k,l}^{\mathrm{t}}$ represent azimuth and zenith AoDs, respectively. The mth element of $\boldsymbol{a}_{\mathrm{r}}$ is denoted by $[\boldsymbol{a}_{\mathrm{r}}(\phi, \theta)]_m \triangleq \frac{1}{\sqrt{N_{\mathrm{rx}}}} \exp(-j\boldsymbol{g}_{\mathrm{r},m}^{\mathrm{T}} \boldsymbol{k}(\phi, \theta))$, $m = 1, 2, \ldots, N_{\mathrm{rx}}$. Similarly, we have $[\boldsymbol{a}_{\mathrm{t}}(\phi, \theta)]_m \triangleq \frac{1}{\sqrt{N_{\mathrm{tx}}}} \exp(-j\boldsymbol{g}_{\mathrm{t},m}^{\mathrm{T}} \boldsymbol{k}(\phi, \theta))$. The $\boldsymbol{g}_{\mathrm{r},m}$ and $\boldsymbol{g}_{\mathrm{t},m}$ are the relative position vectors of the receive and transmit antenna elements with the origin at the center of each array, respectively; $\boldsymbol{k}(\phi, \theta) \triangleq \frac{2\pi}{\lambda}[\cos\phi\sin\theta, \sin\phi\sin\theta, \cos\theta]^{\mathrm{T}}$ is the wave vector, where λ is the wavelength.

C. Signal Model for Pilot Transmission

In the pilot transmission period, N_{BS} BSs employ orthogonal time resources to transmit the pilot symbol sequences. The pilot signal for the nth BS is expressed as [63], [67]

$$s_n^{\mathrm{p}}(t) = \sum_{m=0}^{N_{\mathrm{p}}-1} a_{n,m}^{\mathrm{p}}\, p(t - mT_{\mathrm{s}}) \tag{2}$$

where the pilot symbols in $\{a_{n,0}^{\mathrm{p}}, a_{n,1}^{\mathrm{p}}, \ldots, a_{n,N_{\mathrm{p}}-1}^{\mathrm{p}}\}$ have unit amplitude. The symbol sequence has a length of $N_{\mathrm{p}} \geqslant 1$. The pulse shaping filter $p(t)$ is assumed as an ideal sinc function with power spectral density (PSD) $|P(f)|^2$. From (2), the total training overhead is given by $T_{\mathrm{p}} \triangleq N_{\mathrm{BS}} N_{\mathrm{p}} T_{\mathrm{s}}$, where the symbol duration is denoted by $T_{\mathrm{s}} = 1/B$ with system bandwidth B. Then the received signal at the kth MS from the nth BS is

expressed by

$$\mathbf{y}_{n,k}^{\mathrm{p}}(t) = \sum_{l=1}^{L} \mathbf{H}_{n,k,l} \boldsymbol{F}_n^{\mathrm{p}} (\boldsymbol{P}_n^{\mathrm{p}})^{\frac{1}{2}} \mathbf{1}_{N_{\mathrm{MS}}} s_n^{\mathrm{p}}(t - \tau_{n,k,l}) + \mathbf{n}_k^{\mathrm{p}}(t) \tag{3}$$

$$= \sqrt{N_{\mathrm{rx}} N_{\mathrm{tx}}} \sum_{l=1}^{L} \alpha_{n,k,l} \boldsymbol{a}_{\mathrm{r}}(\varphi_{n,k,l}^{\mathrm{r}}, \theta_{n,k,l}^{\mathrm{r}}) \boldsymbol{a}_{\mathrm{t}}^{\dagger}(\varphi_{n,k,l}^{\mathrm{t}}, \theta_{n,k,l}^{\mathrm{t}})$$

$$\times \boldsymbol{F}_n^{\mathrm{p}} (\boldsymbol{P}_n^{\mathrm{p}})^{\frac{1}{2}} \mathbf{1}_{N_{\mathrm{MS}}} s_n^{\mathrm{p}}(t - \tau_{n,k,l}) + \mathbf{n}_k^{\mathrm{p}}(t) \tag{4}$$

for $t \in ((n-1)N_{\mathrm{p}}T_{\mathrm{s}}, nN_{\mathrm{p}}T_{\mathrm{s}}]$, where $\mathbf{n}_k^{\mathrm{p}}(t)$ is the zero-mean white Gaussian noise vector with i.i.d. random elements following $\mathcal{CN}(0, P_{\mathrm{n}})$. The diagonal matrix $\boldsymbol{P}_n^{\mathrm{p}} \triangleq \mathrm{diag}(p_{n,1}^{\mathrm{p}}, p_{n,2}^{\mathrm{p}}, \ldots, p_{n,N_{\mathrm{MS}}}^{\mathrm{p}})$ represents the power allocation of the nth BS satisfying $\mathrm{Tr}(\boldsymbol{P}_n^{\mathrm{p}}) \leqslant P_{\mathrm{t}}$. The one-vector $\mathbf{1}_{N_{\mathrm{MS}}}$ means that the same pilot symbol is used for all MSs.

D. Signal Model for Data Transmission

In downlink data transmission period, the N_{BS} BSs cooperatively transmit the data streams to the N_{MS} MSs via spatial multiplexing. The data stream transmitted from the BSs to the kth MS is expressed by the symbol sequence with length N_{d} as

$$s_k^{\mathrm{d}}(t) = \sum_{m=0}^{N_{\mathrm{d}}-1} a_{k,m}^{\mathrm{d}} p(t - mT_{\mathrm{s}}) \tag{5}$$

where $a_{k,m}^{\mathrm{d}}$ is a random data symbol, which is assumed to be uncorrelated random variable with zero-mean satisfying $\mathbb{E}\{(a_{k,m}^{\mathrm{d}})^* a_{k',m'}^{\mathrm{d}}\} = \delta(k - k')\delta(m - m')$. The received signal after applying the receive BF can be expressed as

$$y_k^{\mathrm{d}}(t) = \sum_{n=1}^{N_{\mathrm{BS}}} \sum_{l=1}^{L} (\mathbf{w}_k^{\mathrm{d}})^{\dagger} \mathbf{H}_{n,k,l} \mathbf{F}_n^{\mathrm{d}} (\boldsymbol{P}_n^{\mathrm{d}})^{\frac{1}{2}} \mathbf{s}^{\mathrm{d}}(t - \tau_{n,k,l}) + (\mathbf{w}_k^{\mathrm{d}})^{\dagger} \mathbf{n}_k^{\mathrm{d}}(t)$$

$$= \underbrace{\sum_{n=1}^{N_{\mathrm{BS}}} \sum_{l=1}^{L} \sqrt{p_{n,k}^{\mathrm{d}}} (\mathbf{w}_k^{\mathrm{d}})^{\dagger} \mathbf{H}_{n,k,l} \mathbf{f}_{n,k}^{\mathrm{d}} s_k^{\mathrm{d}}(t - \tau_{n,k,l})}_{\text{desired signal}}$$

$$+ \underbrace{\sum_{j=1,j\neq k}^{N_{\mathrm{MS}}} \sum_{n=1}^{N_{\mathrm{BS}}} \sum_{l=1}^{L} \sqrt{p_{n,j}^{\mathrm{d}}} (\mathbf{w}_k^{\mathrm{d}})^{\dagger} \mathbf{H}_{n,k,l} \mathbf{f}_{n,j}^{\mathrm{d}} s_j^{\mathrm{d}}(t - \tau_{n,k})}_{\text{inter-user interference}}$$

$$+ \underbrace{(\mathbf{w}_k^{\mathrm{d}})^{\dagger} \mathbf{n}_k^{\mathrm{d}}(t)}_{\text{noise}} \tag{6}$$

where $\mathbf{s}^{\mathrm{d}}(t) \triangleq [s_1^{\mathrm{d}}(t), s_2^{\mathrm{d}}(t), \ldots, s_{N_{\mathrm{MS}}}^{\mathrm{d}}(t)]^{\mathrm{T}}$. The power allocation for the kth MS at the nth BS is denoted by $p_{n,k}^{\mathrm{d}}$ satisfying $\boldsymbol{P}_n^{\mathrm{d}} \triangleq \mathrm{diag}(p_{n,1}^{\mathrm{d}}, p_{n,2}^{\mathrm{d}}, \ldots, p_{n,N_{\mathrm{MS}}}^{\mathrm{d}})$ with $\mathrm{Tr}(\boldsymbol{P}_n^{\mathrm{d}}) \leqslant P_{\mathrm{t}}$. To express (6) by means of channel estimation error, we define the channel estimation error matrix by [78], [79]

$$\mathbf{E}_{n,k,l} \triangleq \hat{\mathbf{H}}_{n,k,l} - \mathbf{H}_{n,k,l}$$

where $\hat{\mathbf{H}}_{n,k,l}$ is the estimator of $\mathbf{H}_{n,k,l}$ given as

$$\hat{\mathbf{H}}_{n,k,l} \triangleq \sqrt{N_{\mathrm{rx}} N_{\mathrm{tx}}} \hat{\alpha}_{n,k,l} \boldsymbol{a}_{\mathrm{r}}(\hat{\varphi}_{n,k,l}^{\mathrm{r}}, \hat{\theta}_{n,k,l}^{\mathrm{r}}) \boldsymbol{a}_{\mathrm{t}}^{\dagger}(\hat{\varphi}_{n,k,l}^{\mathrm{t}}, \hat{\theta}_{n,k,l}^{\mathrm{t}}). \tag{7}$$

From (6) and (7), the received signal is found to be

$$
\begin{aligned}
y_k^{\mathrm{d}}(t) =& \sum_{n=1}^{N_{\mathrm{BS}}} \sum_{l=1}^{L} \sqrt{p_{n,k}^{\mathrm{d}}} \left(\mathbf{w}_k^{\mathrm{d}}\right)^{\dagger} \widehat{\mathbf{H}}_{n,k,l} \mathbf{f}_{n,k}^{\mathrm{d}} s_k^{\mathrm{d}}(t - \tau_{n,k,l}) \\
&+ \sum_{n=1}^{N_{\mathrm{BS}}} \sum_{\substack{j=1,\\ j \neq k}}^{N_{\mathrm{MS}}} \sum_{l=1}^{L} \sqrt{p_{n,j}^{\mathrm{d}}} \left(\mathbf{w}_k^{\mathrm{d}}\right)^{\dagger} \widehat{\mathbf{H}}_{n,k,l} \mathbf{f}_{n,j}^{\mathrm{d}} s_j^{\mathrm{d}}(t - \tau_{n,k,l}) \\
&- \sum_{n=1}^{N_{\mathrm{BS}}} \sum_{j=1}^{N_{\mathrm{MS}}} \sum_{l=1}^{L} \sqrt{p_{n,j}^{\mathrm{d}}} \left(\mathbf{w}_k^{\mathrm{d}}\right)^{\dagger} \mathbf{E}_{n,k,l} \mathbf{f}_{n,j}^{\mathrm{d}} s_j^{\mathrm{d}}(t - \tau_{n,k,l}) \\
&+ \left(\mathbf{w}_k^{\mathrm{d}}\right)^{\dagger} \mathbf{n}_k^{\mathrm{d}}(t) .
\end{aligned} \tag{8}
$$

III. PERFORMANCE METRIC

A. Localization Accuracy

In the pilot transmission period, we adopt a two-stage estimation procedure described in the following [25], [28]. First, the channel parameters are estimated using the received signals. Then the position and orientation parameters can be obtained by transformation process. We represent the channel parameters between the nth BS and the kth MS by the vector

$$
\boldsymbol{\eta}_{n,k} \triangleq \left[\boldsymbol{\eta}_{n,k,1}^{\mathrm{T}}, \boldsymbol{\eta}_{n,k,2}^{\mathrm{T}}, \cdots, \boldsymbol{\eta}_{n,k,L}^{\mathrm{T}}\right]^{\mathrm{T}} \tag{9}
$$

with

$$
\boldsymbol{\eta}_{n,k,l} \triangleq \left[\varphi_{n,k,l}^{\mathrm{r}}, \theta_{n,k,l}^{\mathrm{r}}, \varphi_{n,k}^{\mathrm{t}}, \theta_{n,k}^{\mathrm{t}}, \tau_{n,k}, \alpha_{n,k}^{(\mathrm{R})}, \alpha_{n,k}^{(\mathrm{I})}\right]^{\mathrm{T}} \tag{10}
$$

where $\alpha_{n,k,l}^{(\mathrm{R})} \triangleq \Re\{\alpha_{n,k,l}\}$ and $\alpha_{n,k,l}^{(\mathrm{I})} \triangleq \Im\{\alpha_{n,k,l}\}$ are the real and imaginary parts of $\alpha_{n,k,l}$, respectively. After estimating $\boldsymbol{\eta}_{n,k}$ for all n and k, the position and orientation parameters (i.e., $\boldsymbol{p}_k^{\mathrm{T}}, \phi_k^{\mathrm{r}}$, and θ_k^{r}) are obtained by transforming (9).

It is known that the mean squared error (MSE) matrix of any unbiased estimator for the deterministic parameters and any estimator of the random parameters is bounded by the inverse of Bayesian Fisher information matrix (FIM) as [80]–[82] [1]

$$
\mathbb{E}\left\{\left(\widehat{\boldsymbol{\eta}}_{n,k} - \boldsymbol{\eta}_{n,k}\right)\left(\widehat{\boldsymbol{\eta}}_{n,k} - \boldsymbol{\eta}_{n,k}\right)^{\mathrm{T}}\right\} \succeq \mathbf{J}_{\boldsymbol{\eta}_{n,k}}^{-1} \tag{11}
$$

where $\mathbf{J}_{\boldsymbol{\eta}_{n,k}} \in \mathbb{R}^{7L \times 7L}$ is the FIM for the unknown $\boldsymbol{\eta}_{n,k}$, which is calculated by [28, eq. (10)] as

$$
[\mathbf{J}_{\boldsymbol{\eta}_{n,k}}]_{i,j} = \frac{1}{P_{\mathrm{n}}} \int_0^{N_{\mathrm{P}} T_{\mathrm{s}}} \Re\left\{\frac{\partial \mathbf{r}_{n,k}^{\dagger}(t)}{\partial [\boldsymbol{\eta}_{n,k}]_i} \frac{\partial \mathbf{r}_{n,k}(t)}{\partial [\boldsymbol{\eta}_{n,k}]_j}\right\} dt . \tag{12}
$$

In (12), the vector $\mathbf{r}_{n,k}(t)$ is the noiseless version of $\mathbf{y}_{n,k}^{\mathrm{p}}(t)$ from (4), which is given as

$$
\begin{aligned}
\mathbf{r}_{n,k}(t) =& \sqrt{N_{\mathrm{rx}} N_{\mathrm{tx}}} \sum_{l=1}^{L} \alpha_{n,k} \boldsymbol{a}_{\mathrm{r}}\left(\varphi_{n,k,l}^{\mathrm{r}}, \theta_{n,k,l}^{\mathrm{r}}\right) \boldsymbol{a}_{\mathrm{t}}^{\dagger}\left(\varphi_{n,k,l}^{\mathrm{t}}, \theta_{n,k,l}^{\mathrm{t}}\right) \\
&\times \boldsymbol{F}_n^{\mathrm{p}} \left(\boldsymbol{P}_n^{\mathrm{p}}\right)^{\frac{1}{2}} \mathbf{1}_{N_{\mathrm{MS}}} s_n^{\mathrm{p}}(t - \tau_{n,k,l}) .
\end{aligned} \tag{13}
$$

Based on (12) and (13), the elements of $\mathbf{J}_{\boldsymbol{\eta}_{n,k}}$ are derived in Appendix A where a simplified notation $\mathsf{J}_{\mathsf{x},\mathsf{y}}$ is used to indicate each element corresponding to the variables x and y. Then Cramér-Rao lower bound (CRLB) of each channel parameter is given by the corresponding diagonal entry of $\mathbf{J}_{\boldsymbol{\eta}_{n,k}}^{-1}$.[2]

---

[1] This is the case when *a priori* probability densities of the parameters are not available, which is a reasonable assumption in mmWave mobile networks.

[2] The use of CRLB as a performance metric for localization is desirable due to its tractability and its asymptotical achievability in high signal-to-noise ratio regimes [19].

1) Asymptotic FIM Approximation: The FIM can be simplified in asymptotic region for large N_{rx}, N_{tx}, and B. It is known that if the number of antennas is large enough, multiple paths from different directions become orthogonal meaning that they do not interfere with each other [83]. Specifically, the off-diagonal sub-matrices of the FIM in (12) can be asymptotically approximated by zero matrices as

$$
\mathbf{J}_{\boldsymbol{\eta}_{n,k}} \approx \begin{bmatrix}
\mathbf{J}_{\boldsymbol{\eta}_{n,k,1}} & \mathbf{0} & \cdots & \mathbf{0} \\
\mathbf{0} & \mathbf{J}_{\boldsymbol{\eta}_{n,k,2}} & \ddots & \mathbf{0} \\
\vdots & \vdots & \ddots & \vdots \\
\mathbf{0} & \mathbf{0} & \cdots & \mathbf{J}_{\boldsymbol{\eta}_{n,k,L}}
\end{bmatrix} . \tag{14}
$$

In (14), each submatrix is also approximated by a block-diagonal structure given in Appendix B when $\boldsymbol{F}_n^{\mathrm{p}}$ includes array steering vectors with large N_{tx}. This can be seen using the results in (55), (56), (58), and (59) of Appendix C. It is worth noting that even with large N_{rx} and B, if N_{tx} is not large enough or $\boldsymbol{F}_n^{\mathrm{p}}$ does not consist of the array steering vectors, the elements of $\mathsf{J}_{\varphi_{n,k,l}^{\mathrm{t}}, \theta_{n,k,l}^{\mathrm{t}}}, \mathsf{J}_{\varphi_{n,k,l}^{\mathrm{t}}, \alpha_{n,k,l}^{(\mathrm{R})}}, \mathsf{J}_{\varphi_{n,k,l}^{\mathrm{t}}, \alpha_{n,k,l}^{(\mathrm{I})}}, \mathsf{J}_{\theta_{n,k,l}^{\mathrm{t}}, \alpha_{n,k,l}^{(\mathrm{R})}}, \mathsf{J}_{\theta_{n,k,l}^{\mathrm{t}}, \alpha_{n,k,l}^{(\mathrm{I})}}$ in (54) may not approach to zero. Since (54) has a special structure, it is possible to calculate the CRLB of each parameter in a closed-form expression using the notation $\mathrm{C}(\cdot)$ as

$$
\mathrm{C}(\widehat{\varphi}_{n,k,l}^{\mathrm{r}}) \approx \left[\left([\mathbf{J}_{\boldsymbol{\eta}_{n,k,l}}]_{1:2,1:2}\right)^{-1}\right]_{1,1} \tag{15a}
$$

$$
\mathrm{C}(\widehat{\theta}_{n,k,l}^{\mathrm{r}}) \approx \left[\left([\mathbf{J}_{\boldsymbol{\eta}_{n,k,l}}]_{1:2,1:2}\right)^{-1}\right]_{2,2} \tag{15b}
$$

$$
\mathrm{C}(\widehat{\varphi}_{n,k,l}^{\mathrm{t}}) \approx \left[\left([\mathbf{J}_{\boldsymbol{\eta}_{n,k,l}}]_{3:4,3:4}\right)^{-1}\right]_{1,1} \tag{15c}
$$

$$
\mathrm{C}(\widehat{\theta}_{n,k,l}^{\mathrm{t}}) \approx \left[\left([\mathbf{J}_{\boldsymbol{\eta}_{n,k,l}}]_{3:4,3:4}\right)^{-1}\right]_{2,2} \tag{15d}
$$

$$
\mathrm{C}(\widehat{\tau}_{n,k,l}) \approx
$$
$$
\left[4\pi^2 B_{\mathrm{eff}}^2 \gamma_{\mathrm{p}} |\alpha_{n,k,l}|^2 \boldsymbol{a}_{\mathrm{t}}^{\dagger}(\varphi_{n,k,l}^{\mathrm{t}}, \theta_{n,k,l}^{\mathrm{t}}) \boldsymbol{V}_n \boldsymbol{a}_{\mathrm{t}}(\varphi_{n,k,l}^{\mathrm{t}}, \theta_{n,k,l}^{\mathrm{t}})\right]^{-1} \tag{15e}
$$

$$
\mathrm{C}(\widehat{\alpha}_{n,k,l}^{(\mathrm{R})}) = \mathrm{C}(\widehat{\alpha}_{n,k,l}^{(\mathrm{I})}) \approx
$$
$$
\left[\gamma_{\mathrm{p}} \boldsymbol{a}_{\mathrm{t}}^{\dagger}(\varphi_{n,k,l}^{\mathrm{t}}, \theta_{n,k,l}^{\mathrm{t}}) \boldsymbol{V}_n \boldsymbol{a}_{\mathrm{t}}(\varphi_{n,k,l}^{\mathrm{t}}, \theta_{n,k,l}^{\mathrm{t}})\right]^{-1} \tag{15f}
$$

where

$$
B_{\mathrm{eff}}^2 \triangleq \int_{-B/2}^{B/2} f^2 |P(f)|^2 df
$$

$$
\gamma_{\mathrm{p}} \triangleq N_{\mathrm{rx}} N_{\mathrm{tx}} N_{\mathrm{p}} / P_{\mathrm{n}}
$$

$$
\boldsymbol{V}_n \triangleq \boldsymbol{F}_n^{\mathrm{p}} \left(\boldsymbol{P}_n^{\mathrm{p}}\right)^{\frac{1}{2}} \mathbf{1}_{N_{\mathrm{MS}} \times N_{\mathrm{MS}}} \left(\boldsymbol{P}_n^{\mathrm{p}}\right)^{\frac{1}{2}} \left(\boldsymbol{F}_n^{\mathrm{p}}\right)^{\dagger} .
$$

It is worth noting that all the inversion operations in (15) can be easily obtained in closed-form expressions as the matrices have the size of 2×2.

2) FIM Transformation for Position and Orientation Parameters: We obtain the squared position error bound (SPEB) and squared orientation error bound (SOEB) for the kth MS by transforming the FIM of $\boldsymbol{\eta}_{n,k}, \forall n$ to that of the position vector, i.e., $\boldsymbol{p}_k = [p_k^{\mathrm{x}}, p_k^{\mathrm{y}}, p_k^{\mathrm{z}}]^{\mathrm{T}}$, and the orientation angles, i.e., $(\phi_k^{\mathrm{r}}, \theta_k^{\mathrm{r}})$. The $(5 + 3N_{\mathrm{BS}}(L-1)) \times 1$ vector containing the position and orientation parameters is defined as

$$
\tilde{\boldsymbol{\eta}}_k \triangleq \left[\boldsymbol{p}_k^{\mathrm{T}}, \phi_k^{\mathrm{r}}, \theta_k^{\mathrm{r}}, \tilde{\boldsymbol{p}}_k\right]^{\mathrm{T}}, k = 1, 2, \ldots, N_{\mathrm{MS}} \tag{16}
$$

where $\tilde{\mathbf{p}}_k \triangleq [\tilde{\mathbf{p}}_{1,k}^{\mathrm{T}}, \tilde{\mathbf{p}}_{2,k}^{\mathrm{T}}, \ldots, \tilde{\mathbf{p}}_{N_{\mathrm{BS}},k}^{\mathrm{T}}]^{\mathrm{T}}$ is a nuisance vector consisting of the positions of $N_{\mathrm{BS}}(L-1)$ NLOS scatterers with $\tilde{\mathbf{p}}_{n,k} \triangleq [\tilde{\mathbf{p}}_{n,k,2}^{\mathrm{T}}, \tilde{\mathbf{p}}_{n,k,3}^{\mathrm{T}} \cdots, \tilde{\mathbf{p}}_{n,k,L}^{\mathrm{T}}]^{\mathrm{T}}$ containing the $L-1$ NLOS positions treating $l=1$ as the LOS path index without loss of generality. Using the transformation technique based on the chain rule and the independent estimations from the N_{BS} BSs, the FIM of $\tilde{\boldsymbol{\eta}}_k$ can be obtained as

$$\mathbf{J}_{\tilde{\boldsymbol{\eta}}_k} = \sum_{n=1}^{N_{\mathrm{BS}}} \mathbf{T}_{n,k} \mathbf{J}_{\boldsymbol{\eta}_{n,k}^{(1)}}^{\mathrm{e}} \mathbf{T}_{n,k}^{\mathrm{T}} \tag{17}$$

where the equivalent FIM (EFIM) of $\boldsymbol{\eta}_{n,k}^{(1)} \triangleq [[\boldsymbol{\eta}_{n,k,1}^{\mathrm{T}}]_{1:5}, [\boldsymbol{\eta}_{n,k,2}^{\mathrm{T}}]_{1:5}, \ldots, [\boldsymbol{\eta}_{n,k,L}^{\mathrm{T}}]_{1:5}]^{\mathrm{T}}$, which only including the parameters related with the position and orientation while excluding $\alpha_{n,k,l}^{(\mathrm{R})}$ and $\alpha_{n,k,l}^{(\mathrm{I})}, \forall l$, is determined by using the Schur complement as [81]

$$\mathbf{J}_{\boldsymbol{\eta}_{n,k}^{(1)}}^{\mathrm{e}} = \mathbf{J}_{\boldsymbol{\eta}_{n,k}^{(1)}} - \mathbf{J}_{\boldsymbol{\eta}_{n,k}^{(1)}, \boldsymbol{\eta}_{n,k}^{(2)}} \mathbf{J}_{\boldsymbol{\eta}_{n,k}^{(2)}}^{-1} \mathbf{J}_{\boldsymbol{\eta}_{n,k}^{(1)}, \boldsymbol{\eta}_{n,k}^{(2)}}^{\mathrm{T}} \tag{18}$$

with $\boldsymbol{\eta}_{n,k}^{(1)} \triangleq [[\boldsymbol{\eta}_{n,k,1}^{\mathrm{T}}]_{1:5}, [\boldsymbol{\eta}_{n,k,2}^{\mathrm{T}}]_{1:5}, \ldots, [\boldsymbol{\eta}_{n,k,L}^{\mathrm{T}}]_{1:5}]^{\mathrm{T}}$ and $\boldsymbol{\eta}_{n,k}^{(2)} \triangleq [[\boldsymbol{\eta}_{n,k,1}^{\mathrm{T}}]_{6:7}, [\boldsymbol{\eta}_{n,k,2}^{\mathrm{T}}]_{6:7}, \ldots, [\boldsymbol{\eta}_{n,k,L}^{\mathrm{T}}]_{6:7}]^{\mathrm{T}}$. In (18), $\mathbf{J}_{\boldsymbol{\eta}_{n,k}^{(1)}, \boldsymbol{\eta}_{n,k}^{(2)}}$ contains the Fisher information between $\boldsymbol{\eta}_{n,k}^{(1)}$ and $\boldsymbol{\eta}_{n,k}^{(2)}$, of which elements can be found from $\mathbf{J}_{\boldsymbol{\eta}_{n,k}}$ in Appendix A. Also, the transformation matrix in (17) is given by

$$\mathbf{T}_{n,k} \triangleq \frac{\partial (\boldsymbol{\eta}_{n,k}^{(1)})^{\mathrm{T}}}{\partial \tilde{\boldsymbol{\eta}}_k} = \begin{bmatrix} \frac{\partial [\boldsymbol{\eta}_{n,k,1}^{\mathrm{T}}]_{1:5}}{\partial \boldsymbol{p}_k} & \cdots & \frac{\partial [\boldsymbol{\eta}_{n,k,L}^{\mathrm{T}}]_{1:5}}{\partial \boldsymbol{p}_k} \\ \frac{\partial [\boldsymbol{\eta}_{n,k,1}^{\mathrm{T}}]_{1:5}}{\partial \phi_k^{\mathrm{r}}} & \cdots & \frac{\partial [\boldsymbol{\eta}_{n,k,L}^{\mathrm{T}}]_{1:5}}{\partial \phi_k^{\mathrm{r}}} \\ \frac{\partial [\boldsymbol{\eta}_{n,k,1}^{\mathrm{T}}]_{1:5}}{\partial \theta_k^{\mathrm{r}}} & \cdots & \frac{\partial [\boldsymbol{\eta}_{n,k,L}^{\mathrm{T}}]_{1:5}}{\partial \theta_k^{\mathrm{r}}} \\ \frac{\partial [\boldsymbol{\eta}_{n,k,1}^{\mathrm{T}}]_{1:5}}{\partial \tilde{\mathbf{p}}_k} & \cdots & \frac{\partial [\boldsymbol{\eta}_{n,k,L}^{\mathrm{T}}]_{1:5}}{\partial \tilde{\mathbf{p}}_k} \end{bmatrix} \tag{19}$$

where $[\boldsymbol{\eta}_{n,k,l}^{\mathrm{T}}]_{1:5} = [\varphi_{n,k,l}^{\mathrm{r}}, \theta_{n,k,l}^{\mathrm{r}}, \varphi_{n,k,l}^{\mathrm{t}}, \theta_{n,k,l}^{\mathrm{t}}, \tau_{n,k,l}]$. The matrix elements in (19) are derived in Appendix D. The EFIM of the position and orientation can be obtained by using the Schur complement of the sub-matrix in $\mathbf{J}_{\tilde{\boldsymbol{\eta}}_k}$ of (17) as

$$\mathbf{J}_{\tilde{\boldsymbol{\eta}}_k^{(1)}}^{\mathrm{e}} = \mathbf{J}_{\tilde{\boldsymbol{\eta}}_k^{(1)}} - \mathbf{J}_{\tilde{\boldsymbol{\eta}}_k^{(1)}, \hat{\boldsymbol{\eta}}_k^{(2)}} \mathbf{J}_{\hat{\boldsymbol{\eta}}_k^{(2)}}^{-1} \mathbf{J}_{\tilde{\boldsymbol{\eta}}_k^{(1)}, \hat{\boldsymbol{\eta}}_k^{(2)}}^{\mathrm{T}} \tag{20}$$

where $\tilde{\boldsymbol{\eta}}_k^{(1)} \triangleq [\boldsymbol{p}_k^{\mathrm{T}}, \phi_k^{\mathrm{r}}, \theta_k^{\mathrm{r}}]^{\mathrm{T}}$ and $\hat{\boldsymbol{\eta}}_k^{(2)} \triangleq \tilde{\mathbf{p}}_k^{\mathrm{T}}$. From (20), the SPEB and SOEB are respectively defined as

$$e_{\mathrm{sp}}^{\ell}\left(\tilde{\boldsymbol{\eta}}_k; N_{\mathrm{p}}, \hat{\boldsymbol{F}}_n^{\mathrm{p}}, \check{\boldsymbol{F}}_n^{\mathrm{p}}, \boldsymbol{P}_n^{\mathrm{p}}\right) = \sum_{i=1}^{3} \left[\left(\mathbf{J}_{\tilde{\boldsymbol{\eta}}_k^{(1)}}^{\mathrm{e}}\right)^{-1} \right]_{i,i} \tag{21}$$

$$e_{\mathrm{so}}^{\ell}\left(\tilde{\boldsymbol{\eta}}_k; N_{\mathrm{p}}, \hat{\boldsymbol{F}}_n^{\mathrm{p}}, \check{\boldsymbol{F}}_n^{\mathrm{p}}, \boldsymbol{P}_n^{\mathrm{p}}\right) = \sum_{i=4}^{5} \left[\left(\mathbf{J}_{\tilde{\boldsymbol{\eta}}_k^{(1)}}^{\mathrm{e}}\right)^{-1} \right]_{i,i}. \tag{22}$$

D. Data Rate

From the received signal model in (6), the effective data rate, which includes the pilot overhead term as a pre-log factor β, is expressed as

$$R = \beta \sum_{k=1}^{N_{\mathrm{MS}}} \log_2 (1 + \gamma_k) \tag{23}$$

with

$$\beta \triangleq 1 - \frac{N_{\mathrm{BS}} N_{\mathrm{p}} T_{\mathrm{s}}}{T_{\mathrm{c}}} \tag{24}$$

$$\gamma_k \triangleq \frac{\left| \sum_{n=1}^{N_{\mathrm{BS}}} \sum_{l=1}^{L} \sqrt{p_{n,k}^{\mathrm{d}}} (\mathbf{w}_k^{\mathrm{d}})^{\dagger} \mathbf{H}_{n,k,l} \mathbf{f}_{n,k}^{\mathrm{d}} \right|^2}{\sum_{j=1, j \neq k}^{N_{\mathrm{MS}}} \left| \sum_{n=1}^{N_{\mathrm{BS}}} \sum_{l=1}^{L} \sqrt{p_{n,j}^{\mathrm{d}}} (\mathbf{w}_k^{\mathrm{d}})^{\dagger} \mathbf{H}_{n,k,l} \mathbf{f}_{n,j}^{\mathrm{d}} \right|^2 + P_{\mathrm{n}} \|\mathbf{w}_k^{\mathrm{d}}\|^2} \tag{25}$$

where $\mathbf{f}_{n,k}^{\mathrm{d}}$ is the kth column of $\mathbf{F}_n^{\mathrm{d}}$ corresponding to the kth MS. In (25), we assume the narrowband system with perfect symbol synchronization where the symbols from N_{BS} BSs are combined without inter-symbol interference.

In reality, the estimated CSI are imperfect. In this case, the BS treats the estimated channels as the true channels in BF design. Then γ_k in (25) can be expressed by treating the inter-user interference and the interference from channel estimation error as a part of the effective noise in (8), which is expressed as (26) shown at the top of the next page [78], [79], [84].

IV. PROPOSED TRANSMISSION SCHEME

In this section, we formulate an optimization problem for designing a cooperative BF and power allocation scheme. In many applications of joint communication and localization systems, it is crucial to guarantee required localization accuracies while providing high data rates for MSs. In this regard, we aim to improve the rate-accuracy region, which is defined as an area of the rate and accuracy that can be simultaneously achievable by joint communication and localization systems with limited wireless resources.

A. Problem Formulation

We consider the accuracy-constrained weighted sum rate maximization problem, from which the area of the rate-accuracy region can be controlled. Unlike the conventional approaches in [67]–[69], the problem formulation here enables flexible beamforming designs for both pilot transmission and data transmission. This can be expressed as a joint optimization problem with multiple control variables, which are grouped in the sets defined by

$$\mathcal{S}_{\mathrm{tx}}^{\mathrm{p}} \triangleq \{N_{\mathrm{p}}, \hat{\boldsymbol{F}}_n^{\mathrm{p}}, \check{\boldsymbol{F}}_n^{\mathrm{p}}, \boldsymbol{P}_n^{\mathrm{p}}\}_{n=1}^{N_{\mathrm{BS}}} \tag{27a}$$

$$\mathcal{S}_{\mathrm{tx}}^{\mathrm{d}} \triangleq \{\hat{\boldsymbol{F}}_n^{\mathrm{d}}, \check{\boldsymbol{F}}_n^{\mathrm{d}}, \boldsymbol{P}_n^{\mathrm{d}}\}_{n=1}^{N_{\mathrm{BS}}} \tag{27b}$$

$$\mathcal{S}_{\mathrm{rx}}^{\mathrm{d}} \triangleq \{\hat{\boldsymbol{W}}_k^{\mathrm{d}}, \check{\boldsymbol{w}}_k^{\mathrm{d}}\}_{k=1}^{N_{\mathrm{MS}}}. \tag{27c}$$

Using (27), the feasible sets for the optimization problem are expressed to consider the constraints as

$$\check{\mathcal{S}}_{\mathrm{tx}}^{\mathrm{p}} \triangleq \left\{ \mathcal{S}_{\mathrm{tx}}^{\mathrm{p}} \colon \mathbb{E} \left\{ e_{\mathrm{sp}}^{\ell}\left(\tilde{\boldsymbol{\eta}}_k; N_{\mathrm{p}}, \hat{\boldsymbol{F}}_n^{\mathrm{p}}, \check{\boldsymbol{F}}_n^{\mathrm{p}}, \boldsymbol{P}_n^{\mathrm{p}}\right) \right\} \leqslant \varepsilon_k^{\mathrm{p}}, \forall k, \tag{28a}$$

$$\mathbb{E} \left\{ e_{\mathrm{so}}^{\ell}\left(\tilde{\boldsymbol{\eta}}_k; N_{\mathrm{p}}, \hat{\boldsymbol{F}}_n^{\mathrm{p}}, \check{\boldsymbol{F}}_n^{\mathrm{p}}, \boldsymbol{P}_n^{\mathrm{p}}\right) \right\} \leqslant \varepsilon_k^{\mathrm{o}}, \forall k, \tag{28b}$$

$$\left| \left[\hat{\boldsymbol{F}}_n^{\mathrm{p}} \right]_{i,j} \right| = 1, \forall n, i, j, \tag{28c}$$

$$\| \hat{\boldsymbol{F}}_n^{\mathrm{p}} \check{\boldsymbol{F}}_n^{\mathrm{p}} \|_{\mathrm{F}}^2 = N_{\mathrm{MS}}, \forall n, \tag{28d}$$

$$\mathrm{Tr}(\boldsymbol{P}_n^{\mathrm{p}}) \leqslant P_{\mathrm{t}}, \forall n, \tag{28e}$$

$$\text{and } \boldsymbol{P}_n^{\mathrm{p}} \succcurlyeq \mathbf{0}, \forall n \right\} \tag{28f}$$

$$\gamma_k = \frac{\left| \sum_{n=1}^{N_{\mathrm{BS}}} \sum_{l=1}^{L} \sqrt{p_{n,k}^{\mathrm{d}}} \left(\mathbf{w}_k^{\mathrm{d}}\right)^\dagger \widehat{\mathbf{H}}_{n,k,l} \mathbf{f}_{n,k}^{\mathrm{d}} \right|^2}{\sum_{\substack{j=1 \\ j \neq k}}^{N_{\mathrm{MS}}} \left| \sum_{n=1}^{N_{\mathrm{BS}}} \sum_{l=1}^{L} \sqrt{p_{n,j}^{\mathrm{d}}} \left(\mathbf{w}_k^{\mathrm{d}}\right)^\dagger \widehat{\mathbf{H}}_{n,k,l} \mathbf{f}_{n,j}^{\mathrm{d}} \right|^2 + \sum_{j=1}^{N_{\mathrm{MS}}} \mathbb{E} \left\{ \left| \sum_{n=1}^{N_{\mathrm{BS}}} \sum_{l=1}^{L} \sqrt{p_{n,j}^{\mathrm{d}}} \left(\mathbf{w}_k^{\mathrm{d}}\right)^\dagger \mathbf{E}_{n,k,l} \mathbf{f}_{n,j}^{\mathrm{d}} \right|^2 \right\} + P_{\mathrm{n}} \|\mathbf{w}_k^{\mathrm{d}}\|^2} \quad (26)$$

$$\check{\mathcal{S}}_{\mathrm{tx}}^{\mathrm{d}} \triangleq \left\{ \mathcal{S}_{\mathrm{tx}}^{\mathrm{d}} : \left| \left[\hat{\boldsymbol{F}}_n^{\mathrm{d}}\right]_{i,j} \right| = 1, \left\| \hat{\boldsymbol{F}}_n^{\mathrm{d}} \check{\boldsymbol{F}}_n^{\mathrm{d}} \right\|_{\mathrm{F}}^2 = N_{\mathrm{MS}}, \right.$$
$$\left. \mathrm{Tr}(\boldsymbol{P}_n^{\mathrm{d}}) \leqslant P_{\mathrm{t}}, \text{ and } \boldsymbol{P}_n^{\mathrm{d}} \succcurlyeq \mathbf{0}, \forall i, j, n \right\} \quad (29)$$

$$\check{\mathcal{S}}_{\mathrm{rx}}^{\mathrm{d}} \triangleq \left\{ \mathcal{S}_{\mathrm{rx}}^{\mathrm{d}} : \left| \left[\hat{\boldsymbol{W}}_k^{\mathrm{d}}\right]_{i,j} \right| = 1, \forall i, j, k \right\}. \quad (30)$$

The constraints in (28a) and (28b) indicate the requirements of the SPEB and SOEB as in [23], [67], where the expectation is taken over the information error ranges of channels, positions, and orientations. The constraint (28c) comes from the use of RF phase shifters at the BSs. The power constraints are satisfied with (28d), (28e), and (28f). The constraint (30) comes from the use of RF phase shifters at the MSs.

From (23), (27), (28), (29), (30), the optimization problem is formulated as

$$\mathcal{P}_0 : \underset{\mathcal{S}_{\mathrm{tx}}^{\mathrm{p}}, \mathcal{S}_{\mathrm{tx}}^{\mathrm{d}}, \mathcal{S}_{\mathrm{rx}}^{\mathrm{d}}}{\text{maximize}} \quad \beta(\mathcal{S}_{\mathrm{tx}}^{\mathrm{p}}) \sum_{k=1}^{N_{\mathrm{MS}}} \zeta_k \log_2 \left(1 + \gamma_k \left(\mathcal{S}_{\mathrm{tx}}^{\mathrm{p}}, \mathcal{S}_{\mathrm{tx}}^{\mathrm{d}}, \mathcal{S}_{\mathrm{rx}}^{\mathrm{d}}\right)\right)$$
$$\text{subject to} \quad \mathcal{S}_{\mathrm{tx}}^{\mathrm{p}} \subseteq \check{\mathcal{S}}_{\mathrm{tx}}^{\mathrm{p}}$$
$$\mathcal{S}_{\mathrm{tx}}^{\mathrm{d}} \subseteq \check{\mathcal{S}}_{\mathrm{tx}}^{\mathrm{d}}$$
$$\mathcal{S}_{\mathrm{rx}}^{\mathrm{d}} \subseteq \check{\mathcal{S}}_{\mathrm{rx}}^{\mathrm{d}}$$

where the weights $\zeta_k, \forall k$ in the objective function can be adjusted during a long-term period to take into account priority among users [85].

Since the pilot transmission and data transmission are separated, Problem $\mathcal{P}_0$ can be decomposed into two subproblems. The first subproblem is for the pilot transmission, in which the SPEB and SOEB requirements are satisfied with minimum pilot length, as follows,

$$\mathcal{P}_1 : \underset{\mathcal{S}_{\mathrm{tx}}^{\mathrm{p}}}{\text{minimize}} \quad N_{\mathrm{p}}(\mathcal{S}_{\mathrm{tx}}^{\mathrm{p}})$$
$$\text{subject to} \quad \mathcal{S}_{\mathrm{tx}}^{\mathrm{p}} \subseteq \check{\mathcal{S}}_{\mathrm{tx}}^{\mathrm{p}}$$

where the objective is to maximize the data rate by reducing the pilot overhead. After solving Problem $\mathcal{P}_1$ at a centralized unit, the pilot signals are transmitted from the BSs. After the pilot transmission, the BSs are assumed to have the imperfect CSI through the estimation techniques [86], [87]. Then the second subproblem is solved for data transmission, where the weighted sum rate of the MSs is maximized using the estimated CSI as follows,

$$\mathcal{P}_2 : \underset{\mathcal{S}_{\mathrm{tx}}^{\mathrm{d}}, \mathcal{S}_{\mathrm{rx}}^{\mathrm{d}}}{\text{maximize}} \quad \sum_{k=1}^{N_{\mathrm{MS}}} \zeta_k \log_2 \left(1 + \gamma_k \left(\mathcal{S}_{\mathrm{tx}}^{\mathrm{d}}, \mathcal{S}_{\mathrm{rx}}^{\mathrm{d}}\right)\right)$$
$$\text{subject to} \quad \mathcal{S}_{\mathrm{tx}}^{\mathrm{d}} \subseteq \check{\mathcal{S}}_{\mathrm{tx}}^{\mathrm{d}}$$
$$\mathcal{S}_{\mathrm{rx}}^{\mathrm{d}} \subseteq \check{\mathcal{S}}_{\mathrm{rx}}^{\mathrm{d}}.$$

According to the decomposed problems $\mathcal{P}_1$ and $\mathcal{P}_2$, we develop a two-stage design method as presented in the following subsections.

B. Stage I: Beamforming and Power Allocation for Pilot Transmission

Since Problem $\mathcal{P}_1$ is a mixed-integer problem with non-convex constraints, it is difficult to directly solve. Instead, we simplify Problem $\mathcal{P}_1$ by fixing the pilot BF matrices and design an iterative pilot power allocation algorithm. In other words, design of Stage I consists of two steps, where the first step is for pilot BF while the second step is for pilot power allocation.

1) GNSS-Aided BF for Pilot Transmission: Before channel estimation, the knowledge of the CSI is unavailable. In this case, design of sophisticated beamforming is difficult due to the lack of the instantaneous CSI. Alternatively, we rely on the RF-only beamforming such that $\boldsymbol{F}_n^{\mathrm{p}} = \hat{\boldsymbol{F}}_n^{\mathrm{p}}$ and $\check{\boldsymbol{F}}_n^{\mathrm{p}} = \boldsymbol{I}$. The matrix $\hat{\boldsymbol{F}}_n^{\mathrm{p}}$ is designed by using only the information of AoD from the BSs to the MSs. We consider that the AoD can be extracted from the GNSS information sent from the MSs or by exploiting the existing beam tracking techniques. For more realistic systems, inaccurate GNSS information of the MSs are used for $\hat{\boldsymbol{F}}_n^{\mathrm{p}}$. To be specific, the kth column vector of $\hat{\boldsymbol{F}}_n^{\mathrm{p}}$ is determined by the array steering vector with the AoD between the nth BS and the kth MS based on the GNSS information as follows,

$$\boldsymbol{F}_n^{\mathrm{p}} = \hat{\boldsymbol{F}}_n^{\mathrm{p}} = \left[\boldsymbol{a}_{\mathrm{t}} \left(\tilde{\varphi}_{n,1}^{\mathrm{t}}, \tilde{\theta}_{n,1}^{\mathrm{t}}\right) \middle| \cdots \middle| \boldsymbol{a}_{\mathrm{t}} \left(\tilde{\varphi}_{n,N_{\mathrm{MS}}}^{\mathrm{t}}, \tilde{\theta}_{n,N_{\mathrm{MS}}}^{\mathrm{t}}\right) \right], \forall n \quad (31)$$

where $(\tilde{\varphi}_{n,k}^{\mathrm{t}}, \tilde{\theta}_{n,k}^{\mathrm{t}})$ represent the AoD of the nth BS corresponding to the GNSS information of the kth MS, which are assumed to be inaccurate.

2) Pilot Length and Power Allocation for Pilot Transmission: After fixing $\boldsymbol{F}_n^{\mathrm{p}}$ as in (31), $\mathcal{P}_1$ reduces to

$$\mathcal{P}_{1,\mathrm{a}} : \underset{\mathcal{S}_{\mathrm{tx}}^{\mathrm{p,a}}}{\text{minimize}} \quad N_{\mathrm{p}} \left(\mathcal{S}_{\mathrm{tx}}^{\mathrm{p,a}}\right)$$
$$\text{subject to} \quad \mathcal{S}_{\mathrm{tx}}^{\mathrm{p,a}} \subseteq \check{\mathcal{S}}_{\mathrm{tx}}^{\mathrm{p,a}}$$

where $\mathcal{S}_{\mathrm{tx}}^{\mathrm{p,a}} \triangleq \{N_{\mathrm{p}}, \hat{\boldsymbol{F}}_n^{\mathrm{p}}, \boldsymbol{P}_n^{\mathrm{p}}\}_{n=1}^{N_{\mathrm{BS}}}$. The set $\check{\mathcal{S}}_{\mathrm{tx}}^{\mathrm{p,a}}$ is defined similarly with $\check{\mathcal{S}}_{\mathrm{tx}}^{\mathrm{p}}$ in (28) as

$$\check{\mathcal{S}}_{\mathrm{tx}}^{\mathrm{p,a}} \triangleq \{\mathcal{S}_{\mathrm{tx}}^{\mathrm{p,a}} : \text{(28a), (28b), (28e), (28f), and (31)}\}. \quad (32)$$

Since $\boldsymbol{P}_n^{\mathrm{p}}$ does not affect the objective function, the optimal solution to Problem $\mathcal{P}_{1,\mathrm{a}}$ can be obtained by solving an outer-inner problem, where the outer problem is to find the minimum N_{p} which can give feasible solutions of $\boldsymbol{P}_n^{\mathrm{p}}$ to the inner problem satisfying all constraints. The inner problem is expressed for a given $N_{\mathrm{p}} = \tilde{N}_{\mathrm{p}}$ as

$$\mathcal{P}_{1,\mathrm{b}} : \underset{\mathcal{S}_{\mathrm{tx}}^{\mathrm{p,b}}}{\text{minimize}} \quad 0$$
$$\text{subject to} \quad \mathcal{S}_{\mathrm{tx}}^{\mathrm{p,b}} \subseteq \check{\mathcal{S}}_{\mathrm{tx}}^{\mathrm{p,b}}$$

where $\mathcal{S}_{\mathrm{tx}}^{\mathrm{p,b}} \triangleq \{N_{\mathrm{p}}, \hat{\boldsymbol{F}}_n^{\mathrm{p}}, \boldsymbol{P}_n^{\mathrm{p}}\}_{n=1}^{N_{\mathrm{BS}}}$. The set $\check{\mathcal{S}}_{\mathrm{tx}}^{\mathrm{p,b}}$ is defined as

$$\check{\mathcal{S}}_{\mathrm{tx}}^{\mathrm{p,b}} \triangleq \left\{ \mathcal{S}_{\mathrm{tx}}^{\mathrm{p,b}} : \text{(28a), (28b), (28e), (28f), (31), and } N_{\mathrm{p}} = \tilde{N}_{\mathrm{p}} \right\}.$$
(33)

Problem $\mathscr{P}_{1,\mathrm{b}}$ with zero objective is a standard formula for feasibility problem [88].

Since the functions $e_{\mathrm{sp}}^{\ell}(\tilde{\boldsymbol{\eta}}_k; N_{\mathrm{p}}, \hat{\boldsymbol{F}}_n^{\mathrm{p}}, \check{\boldsymbol{F}}_n^{\mathrm{p}}, \boldsymbol{P}_n^{\mathrm{p}})$ and $e_{\mathrm{so}}^{\ell}(\tilde{\boldsymbol{\eta}}_k; N_{\mathrm{p}}, \hat{\boldsymbol{F}}_n^{\mathrm{p}}, \check{\boldsymbol{F}}_n^{\mathrm{p}}, \boldsymbol{P}_n^{\mathrm{p}})$ in (28a) and (28b) are inversely proportional to N_{p}, respectively, we can find the optimal N_{p} of the outer problem by using the bisection method where the inner problem is solved for each outer iteration. To solve the inner problem, we need to deal with the expectation over the information error ranges in the constraints (28a) and (28b). However, the exact probability distributions of the error ranges of channels, positions, and orientations are unknown for an arbitrary MS. Instead, we adopt the sample average approximation method as in [68, eq. (21)] to calculate the expectations for given $\boldsymbol{F}_n^{\mathrm{p}}$ as

$$\mathbb{E}\left\{e_{\mathrm{sp}}^{\ell}(\tilde{\boldsymbol{\eta}}_k; N_{\mathrm{p}}, \hat{\boldsymbol{F}}_n^{\mathrm{p}}, \check{\boldsymbol{F}}_n^{\mathrm{p}}, \boldsymbol{P}_n^{\mathrm{p}})\right\} \approx \frac{1}{N_{\mathrm{sa}}} \sum_{i=1}^{N_{\mathrm{sa}}} \sum_{j=1}^{3} \left[\left(\boldsymbol{J}_{\tilde{\boldsymbol{\eta}}_{k,i}^{(1)}}^{\mathrm{e}}\right)^{-1}\right]_{j,j}$$
(34a)

$$\mathbb{E}\left\{e_{\mathrm{so}}^{\ell}(\tilde{\boldsymbol{\eta}}_k; N_{\mathrm{p}}, \hat{\boldsymbol{F}}_n^{\mathrm{p}}, \check{\boldsymbol{F}}_n^{\mathrm{p}}, \boldsymbol{P}_n^{\mathrm{p}})\right\} \approx \frac{1}{N_{\mathrm{sa}}} \sum_{i=1}^{N_{\mathrm{sa}}} \sum_{j=4}^{5} \left[\left(\boldsymbol{J}_{\tilde{\boldsymbol{\eta}}_{k,i}^{(1)}}^{\mathrm{e}}\right)^{-1}\right]_{j,j}$$
(34b)

where N_{sa} is the number of samples. $\tilde{\boldsymbol{\eta}}_{k,i}^{(1)}$ is the ith sample of $\tilde{\boldsymbol{\eta}}_k^{(1)}$ in (20). Specifically, the position and orientation parameters are uniformly sampled within the information error ranges. In addition, we only use the dominant LOS paths in calculating (34a) and (34b), which can be thought of as the worst-case performance because multi-path components independently contribute to the FIM as N_{rx} and B increase [28]. For the ith sample, the AoDs and AoAs of N_{BS} LOS paths and $\bar{H}_{n,k}^{(\mathrm{L})}$ can be determined according to the geometric relationship between those parameters and sampled position and orientation. Also, the ith sample for $\boldsymbol{\alpha}_{n,k,1}$ denoted by $\alpha_{n,k,1}^{(i)}$ is obtained according to the known distribution, i.e., $\mathcal{CN}(0, (\bar{H}_{n,k}^{(\mathrm{L})})^2)$. Consequently, using (17), (18), and (20), the EFIM in (34a) and (34b) is approximated as

$$\boldsymbol{J}_{\tilde{\boldsymbol{\eta}}_{k,i}^{(1)}}^{\mathrm{e}} \approx \sum_{n=1}^{N_{\mathrm{BS}}} [\boldsymbol{T}_{n,k}]_{1:5,1:5} \, \boldsymbol{J}_{[\boldsymbol{\eta}_{n,k,1,i}]_{1:5}} \, [\boldsymbol{T}_{n,k}^{\mathrm{T}}]_{1:5,1:5}$$
(35)

where $\boldsymbol{\eta}_{n,k,1,i}$ is the ith sample of $\boldsymbol{\eta}_{n,k,1}$ in (10). It is worth noting that by substituting (34a), (34b), and (35) into the constraints (28a) and (28b), the constraint sets become convex with respect to $(\boldsymbol{P}_n^{\mathrm{p}})^{\frac{1}{2}}$. Then the inner problem $\mathscr{P}_{1,\mathrm{b}}$ can be approximated by re-defining the constraint set $\check{\mathcal{S}}_{\mathrm{tx}}^{\mathrm{p,b}}$ as

$$\check{\mathcal{S}}_{\mathrm{tx}}^{\mathrm{p,b}} \triangleq \left\{ \mathcal{S}_{\mathrm{tx}}^{\mathrm{p,b}} : \frac{1}{N_{\mathrm{sa}}} \sum_{i=1}^{N_{\mathrm{sa}}} \sum_{j=1}^{3} \left[\left(\boldsymbol{J}_{\tilde{\boldsymbol{\eta}}_{k,i}^{(1)}}^{\mathrm{e}}\right)^{-1}\right]_{j,j} \leqslant \varepsilon_k^{\mathrm{p}}, \forall k, \right.$$

$$\left. \frac{1}{N_{\mathrm{sa}}} \sum_{i=1}^{N_{\mathrm{sa}}} \sum_{j=4}^{5} \left[\left(\boldsymbol{J}_{\tilde{\boldsymbol{\eta}}_{k,i}^{(1)}}^{\mathrm{e}}\right)^{-1}\right]_{j,j} \leqslant \varepsilon_k^{\mathrm{o}}, \forall k, \right.$$

Algorithm 1: Joint optimization of pilot length and pilot power allocation

Require: $P_{\mathrm{t}}, \boldsymbol{F}_n^{\mathrm{p}}, \forall n$
1:   $(N_{\mathrm{p}}^{\mathrm{lo}}, N_{\mathrm{p}}^{\mathrm{up}}) \leftarrow (1, N_{\mathrm{p}}^{\mathrm{max}})^3$
2:   **while** N_{p} does not converge within max iteration **do**
3:     $N_{\mathrm{p}} \leftarrow (N_{\mathrm{p}}^{\mathrm{lo}} + N_{\mathrm{p}}^{\mathrm{up}})/2$
4:     $\boldsymbol{P}_n^{\mathrm{p}} \leftarrow$ Solving Problem $\mathscr{P}_{1,\mathrm{b}}$ with substituting (36)
5:     **if** (34a) and (34b) satisfy (28a) and (28b) **then**
6:       $N_{\mathrm{p}}^{\mathrm{up}} \leftarrow N_{\mathrm{p}}$
7:     **else**
8:       $N_{\mathrm{p}}^{\mathrm{lo}} \leftarrow N_{\mathrm{p}}$
9:     **end if**
10:   **end while**
    Return: $N_{\mathrm{p}}, \boldsymbol{P}_n^{\mathrm{p}}, \forall n$

$$\left. \text{(28e), (28f), (31), and } N_{\mathrm{p}} = \tilde{N}_{\mathrm{p}} \right\} \quad (36)$$

where $\boldsymbol{J}_{\tilde{\boldsymbol{\eta}}_{k,i}^{(1)}}^{\mathrm{e}}$ is calculated using (35). Then Problem $\mathscr{P}_{1,\mathrm{b}}$ using (36) can be efficiently solved for $(\boldsymbol{P}_n^{\mathrm{p}})^{\frac{1}{2}}$ by using the existing solver, e.g., interior-point method. The proposed algorithm for joint optimization of pilot length and pilot power allocation is summarized in Algorithm 1.

C. Stage II: Beamforming and Power Allocation for Data Transmission

The main challenge in solving Problem $\mathscr{P}_2$ is to jointly design the RF and baseband BF matrices for the BSs and MSs in the network. Since joint optimization of the matrices is highly complicated in cooperative networks, we adopt the two-step BF approach, which has been widely used for hybrid BF design [89], [90]. After the RF BF matrices are determined in the first step, the baseband BF and power allocation are optimized for the effective channels in the second step.

1) RF BF for Data Transmission: After the pilot transmission, the BSs and MSs have the estimates of the channel parameters. Then the RF BF matrices for data transmission are firstly determined using the estimates of the AoDs and AoAs for the LOS paths and for all n and k as [89]

$$\hat{\mathbf{F}}_n^{\mathrm{d}} = \left[\boldsymbol{a}_{\mathrm{t}}(\hat{\varphi}_{n,1,1}^{\mathrm{t}}, \hat{\theta}_{n,1,1}^{\mathrm{t}}) | \cdots | \boldsymbol{a}_{\mathrm{t}}(\hat{\varphi}_{n,N_{\mathrm{MS}},1}^{\mathrm{t}}, \hat{\theta}_{n,N_{\mathrm{MS}},1}^{\mathrm{t}})\right] \quad (37)$$

$$\hat{\mathbf{W}}_k^{\mathrm{d}} = \left[\boldsymbol{a}_{\mathrm{r}}(\hat{\varphi}_{1,k,1}^{\mathrm{r}}, \hat{\theta}_{1,k,1}^{\mathrm{r}}) | \cdots | \boldsymbol{a}_{\mathrm{r}}(\hat{\varphi}_{N_{\mathrm{BS}},k,1}^{\mathrm{r}}, \hat{\theta}_{N_{\mathrm{BS}},k,1}^{\mathrm{r}})\right] \quad (38)$$

where notation $\hat{x}$ represents the estimated version of x. Then the baseband BF matrices $\check{\mathbf{F}}_n^{\mathrm{d}}$ are designed with transmit power allocation $\mathbf{P}_n^{\mathrm{d}}$ at the BSs while $\check{\boldsymbol{w}}_k^{\mathrm{d}} = \mathbf{1}_{N_{\mathrm{BS}}}$ is used for baseband combining at the MSs.

Using (37) and (38) in (26), we analyze the achievable rate of the kth MS. For large number of antennas (N_{tx} and N_{rx}) and perfect location information, (26) can be upper bounded as

$$\gamma_k \leqslant \tilde{\gamma}_k$$

---

[3]N_{max} is the maximum possible N_{p} within the channel coherence time T_{c}. $N_{\mathrm{p}}^{\mathrm{lo}}$ and $N_{\mathrm{p}}^{\mathrm{up}}$ are used for bisection method.

where

$$\tilde{\gamma}_k \triangleq \frac{\left| \sum_{n=1}^{N_{\text{BS}}} \sum_{l=1}^{L} \sqrt{p_{n,k}^{\text{d}}} \mathbf{w}_k^{\dagger} \widehat{\mathbf{H}}_{n,k,l} \mathbf{f}_{n,k}^{\text{d}} \right|^2}{\sum_{\substack{j=1, \\ j \neq k}}^{N_{\text{MS}}} \left| \sum_{n=1}^{N_{\text{BS}}} \sum_{l=1}^{L} \sqrt{p_{n,j}^{\text{d}}} \mathbf{w}_k^{\dagger} \widehat{\mathbf{H}}_{n,k,l} \mathbf{f}_{n,j}^{\text{d}} \right|^2 + \frac{2P_{\text{n}}}{N_{\text{P}}} \sum_{n=1}^{N_{\text{BS}}} \frac{p_{n,k}^{\text{d}}}{p_{n,k}^{\text{P}}} + P_{\text{n}} \|\mathbf{w}_k\|^2}.$$

(39)

The proof for the above inequality is given in Appendix E. In (39), we see that the achievable rate of the kth MS is affected by the quality of the channel gain estimation for the kth MS rather than those for other MSs when N_{tx} and N_{rx} are large.

2) Baseband BF and Power Allocation for Data Transmission: After fixing the RF BF matrices, the baseband BF and power allocation for the BSs are optimized by solving the following cooperative BF problem,

$$\mathscr{P}_{2,\text{a}}: \underset{\mathcal{S}_{\text{tx}}^{\text{d,a}}, \mathcal{S}_{\text{rx}}^{\text{d,a}}}{\text{maximize}} \quad \sum_{k=1}^{N_{\text{MS}}} \zeta_k \log_2 \left(1 + \tilde{\gamma}_k \left(\mathcal{S}_{\text{tx}}^{\text{d,a}}, \mathcal{S}_{\text{rx}}^{\text{d,a}} \right) \right)$$

$$\text{subject to} \quad \mathcal{S}_{\text{tx}}^{\text{d,a}} \subseteq \check{\mathcal{S}}_{\text{tx}}^{\text{d,a}}$$

$$\mathcal{S}_{\text{rx}}^{\text{d,a}} \subseteq \check{\mathcal{S}}_{\text{rx}}^{\text{d,a}}$$

where $\mathcal{S}_{\text{tx}}^{\text{d,a}} \triangleq \{\hat{\boldsymbol{F}}_n^{\text{d}}, \check{\boldsymbol{F}}_n^{\text{d}}, \boldsymbol{P}_n^{\text{d}}\}_{n=1}^{N_{\text{BS}}}$ and $\mathcal{S}_{\text{rx}}^{\text{d,a}} \triangleq \{\hat{\boldsymbol{W}}_k^{\text{d}}\}_{k=1}^{N_{\text{MS}}}$. The set $\check{\mathcal{S}}_{\text{tx}}^{\text{d,a}}$ and $\check{\mathcal{S}}_{\text{rx}}^{\text{d,a}}$ are defined as

$$\check{\mathcal{S}}_{\text{tx}}^{\text{d,a}} \triangleq \Big\{ \mathcal{S}_{\text{tx}}^{\text{d,a}} : \|\hat{\boldsymbol{F}}_n^{\text{d}} \check{\boldsymbol{F}}_n^{\text{d}}\|_{\text{F}}^2 = N_{\text{MS}}, \text{Tr}(\boldsymbol{P}_n^{\text{d}}) \leqslant P_{\text{t}},$$

$$\boldsymbol{P}_n^{\text{d}} \succcurlyeq \boldsymbol{0}, \forall n, \text{ and } (37) \Big\}. \quad (40)$$

$$\check{\mathcal{S}}_{\text{rx}}^{\text{d,a}} \triangleq \big\{ \mathcal{S}_{\text{rx}}^{\text{d,a}} : (38) \big\}. \quad (41)$$

To solve Problem $\mathscr{P}_{2,\text{a}}$, the BF and power allocation variables are merged and re-organized by introducing the power scaling vector which is common for all BSs [76]. Since the approach using a common power scaling vector is useful to control the desired signal power and interference power from the neighboring BSs, it can provide a sub-optimal solution to the non-convex optimization problem for cooperative BF design. Specifically, we alternate the two procedures, i.e., the baseband BF update and power scaling update, which solve the corresponding sub-problems. Besides, we consider the effect of channel estimation error based on the expression in (39).

In the first subproblem, for notational brevity, we define two vectors as $\bar{\boldsymbol{h}}_{k,j} \triangleq [\sqrt{p_{1,j}^{\text{d}}} \sum_{l=1}^{L} \boldsymbol{w}_k^{\dagger} \widehat{\boldsymbol{H}}_{1,k,l} \hat{\boldsymbol{F}}_1^{\text{d}} | \cdots | \sqrt{p_{N_{\text{BS}},j}^{\text{d}}} \sum_{l=1}^{L} \boldsymbol{w}_k^{\dagger} \widehat{\boldsymbol{H}}_{N_{\text{BS}},k,l} \hat{\boldsymbol{F}}_{N_{\text{BS}}}^{\text{d}}]^{\text{T}}$ and $\bar{\boldsymbol{f}}_k \triangleq [(\check{\boldsymbol{f}}_{1,k}^{\text{d}})^{\text{T}} | \cdots | (\check{\boldsymbol{f}}_{N_{\text{BS}},k}^{\text{d}})^{\text{T}}]^{\text{T}}$. Using these vector notations, $\tilde{\gamma}_k$ can be expressed by

$$\tilde{\gamma}_k = \frac{|\bar{\boldsymbol{h}}_{k,k}^{\text{T}} \bar{\boldsymbol{f}}_k|^2}{\sum_{j=1, j \neq k}^{N_{\text{MS}}} |\bar{\boldsymbol{h}}_{k,j}^{\text{T}} \bar{\boldsymbol{f}}_j|^2 + \frac{2P_{\text{n}}}{N_{\text{P}}} \sum_{n=1}^{N_{\text{BS}}} \frac{p_{n,k}^{\text{d}}}{p_{n,k}^{\text{P}}} + P_{\text{n}} \|\boldsymbol{w}_k\|^2}. \quad (42)$$

Using (42), the baseband BF problem is formulated for a given $\boldsymbol{P}_n^{\text{d}} = \tilde{\boldsymbol{P}}_n^{\text{d}}$ as

$$\mathscr{P}_{2,\text{b}}: \underset{\mathcal{S}_{\text{tx}}^{\text{d,b}}}{\text{maximize}} \quad \sum_{k=1}^{N_{\text{MS}}} \zeta_k \log_2 \left(1 + \tilde{\gamma}_k \left(\mathcal{S}_{\text{tx}}^{\text{d,b}} \right) \right)$$

$$\text{subject to} \quad \mathcal{S}_{\text{tx}}^{\text{d,b}} \subseteq \check{\mathcal{S}}_{\text{tx}}^{\text{d,b}}$$

where $\mathcal{S}_{\text{tx}}^{\text{d,b}} \triangleq \{\bar{\boldsymbol{h}}_{k,j}, \forall j, \bar{\boldsymbol{f}}_k\}_{k=1}^{N_{\text{MS}}}$. The set $\check{\mathcal{S}}_{\text{tx}}^{\text{d,b}}$ is defined as

$$\check{\mathcal{S}}_{\text{tx}}^{\text{d,b}} \triangleq \Big\{ \mathcal{S}_{\text{tx}}^{\text{d,b}} : \|\text{blkdiag}(\hat{\boldsymbol{F}}_1^{\text{d}}, \hat{\boldsymbol{F}}_2^{\text{d}}, \dots, \hat{\boldsymbol{F}}_{N_{\text{BS}}}^{\text{d}}) \bar{\boldsymbol{f}}_k\|^2 = 1, \forall k$$

$$(37), (38), \text{ and } \boldsymbol{P}_n^{\text{d}} = \tilde{\boldsymbol{P}}_n^{\text{d}} \Big\} \quad (43)$$

which is to satisfy the power normalization for each MS, where $\text{blkdiag}(\cdot)$ constitutes a block diagonal matrix. To solve Problem $\mathscr{P}_{2,\text{b}}$, we apply [76, Algorithm 1] in which the same notations are used by defining the effective noise power $\sigma_k^2 \triangleq \frac{2P_{\text{n}}}{N_{\text{P}}} \sum_{n=1}^{N_{\text{BS}}} \frac{p_{n,k}^{\text{d}}}{p_{n,k}^{\text{P}}} + P_{\text{n}} \|\boldsymbol{w}_k\|^2$ and the two matrices $\boldsymbol{A}_k \triangleq \zeta_k / \log 2 / (\sum_{j=1}^{N_{\text{MS}}} |\bar{\boldsymbol{h}}_{k,j}^{\text{T}} \bar{\boldsymbol{f}}_j|^2 + \sigma_k^2) \bar{\boldsymbol{h}}_{k,k} \bar{\boldsymbol{h}}_{k,k}^{\dagger}$ and $\boldsymbol{B}_k \triangleq \sum_{j \neq k} \gamma_j \zeta_j / \log 2 / (\sum_{i=1}^{N_{\text{MS}}} |\bar{\boldsymbol{h}}_{j,i}^{\text{T}} \bar{\boldsymbol{f}}_i|^2 + \sigma_j^2) \bar{\boldsymbol{h}}_{j,k} \bar{\boldsymbol{h}}_{j,k}^{\dagger}$. Specifically, the solution to Problem $\mathscr{P}_{2,\text{b}}$ is obtained by iteratively solving the following problem for each k,

$$\underset{\bar{\boldsymbol{f}}_k}{\text{maximize}} \quad \bar{\boldsymbol{f}}_k^{\dagger} (\boldsymbol{A}_k - \boldsymbol{B}_k) \bar{\boldsymbol{f}}_k \quad (44\text{a})$$

$$\text{subject to} \quad \|\text{blkdiag}(\hat{\boldsymbol{F}}_1^{\text{d}}, \hat{\boldsymbol{F}}_2^{\text{d}}, \dots, \hat{\boldsymbol{F}}_{N_{\text{BS}}}^{\text{d}}) \bar{\boldsymbol{f}}_k\|^2 = 1. \quad (44\text{b})$$

The problem in (44) can be solved by choosing the dominant eigenvector of the updated $\boldsymbol{A}_k - \boldsymbol{B}_k$ in each iteration. Let the eigenvalue decomposition be $\boldsymbol{A}_k - \boldsymbol{B}_k = \boldsymbol{U}_k \boldsymbol{\Sigma}_k \boldsymbol{U}_k^{\text{H}}$ with $\boldsymbol{U}_k \triangleq [\boldsymbol{u}_{k,1} | \boldsymbol{u}_{k,2} | \cdots | \boldsymbol{u}_{k,N_{\text{BS}} N_{\text{MS}}}]$, where the diagonal matrix $\boldsymbol{\Sigma}_k$ has the eigenvalues in descending order. Then the solution to the problem in (44) can be expressed as

$$\bar{\boldsymbol{f}}_k = \frac{\boldsymbol{u}_{k,1}}{\|\text{blkdiag}(\hat{\boldsymbol{F}}_1^{\text{d}}, \hat{\boldsymbol{F}}_2^{\text{d}}, \dots, \hat{\boldsymbol{F}}_{N_{\text{BS}}}^{\text{d}}) \boldsymbol{u}_{k,1}\|}. \quad (45)$$

In the second subproblem, $\tilde{\gamma}_k$ is expressed by introducing the power scaling factor $\bar{p}_k$ for given $\bar{\boldsymbol{f}}_k$ as

$$\tilde{\gamma}_k = \frac{g_{k,k} \bar{p}_k}{\sum_{j=1, j \neq k}^{N_{\text{MS}}} g_{k,j} \bar{p}_j + a_k \bar{p}_k + P_{\text{n}} \|\boldsymbol{w}_k\|^2} \quad (46)$$

where

$$g_{k,j} \triangleq \left| \sum_{n=1}^{N_{\text{BS}}} \sum_{l=1}^{L} \boldsymbol{w}_k^{\dagger} \widehat{\boldsymbol{H}}_{n,k} \boldsymbol{f}_{n,j}^{\text{d}} \right|^2$$

$$a_k \triangleq \frac{2P_{\text{n}}}{N_{\text{P}}} \sum_{n=1}^{N_{\text{BS}}} \frac{\|\boldsymbol{f}_{n,k}^{\text{d}}\|^2}{p_{n,k}^{\text{P}}}.$$

Using (46), the power allocation problem is formulated for given $g_{k,j} = \tilde{g}_{k,j}$ and $a_k = \tilde{a}_k$ as

$$\mathscr{P}_{2,\text{c}}: \underset{\mathcal{S}_{\text{tx}}^{\text{d,c}}}{\text{maximize}} \quad \sum_{k=1}^{N_{\text{MS}}} \zeta_k \log_2 \left(1 + \tilde{\gamma}_k \left(\mathcal{S}_{\text{tx}}^{\text{d,c}} \right) \right)$$

$$\text{subject to} \quad \mathcal{S}_{\text{tx}}^{\text{d,c}} \subseteq \check{\mathcal{S}}_{\text{tx}}^{\text{d,c}}$$

where $\mathcal{S}_{\text{tx}}^{\text{d,c}} \triangleq \{g_{k,j}, a_k, \bar{p}_k\}_{k=1}^{N_{\text{MS}}}$. The set $\check{\mathcal{S}}_{\text{tx}}^{\text{d,c}}$ is defined as

$$\check{\mathcal{S}}_{\text{tx}}^{\text{d,c}} \triangleq \Big\{ \mathcal{S}_{\text{tx}}^{\text{d,c}} : \sum_{k=1}^{N_{\text{MS}}} \left\| \hat{\boldsymbol{F}}_n^{\text{d}} \check{\boldsymbol{f}}_{n,k}^{\text{d}} \right\|^2 \bar{p}_k \leqslant P_{\text{t}}, \bar{p}_k \geqslant 0, \forall n, k$$

$$g_{k,j} = \tilde{g}_{k,j}, \text{ and } a_k = \tilde{a}_k, \forall j, k \Big\} \quad (48)$$

We find a local optimal solution to Problem $\mathscr{P}_{2,\text{c}}$ based on the Karush-Kuhn-Tucker (KKT) conditions. To this end, we express
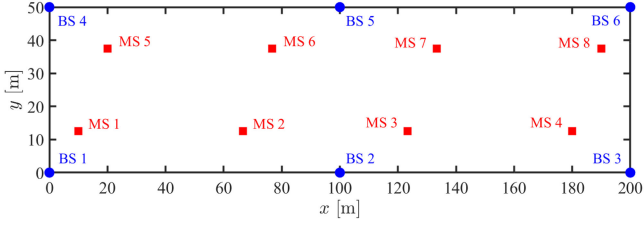
Fig. 2. Network geometry with $N_{\mathrm{BS}} = 6$ and $N_{\mathrm{MS}} = 8$. The GNSS position information have random errors within 1 m radius in the x-y plane. The UPAs of the BSs are down-tilted by $\theta_n^{\mathrm{t}} = 30^{\mathrm{o}}$ from the x-z plane to the direction of the ground. The arrays of MS 1-MS 4 are oriented to the $+x$-axis while that of MS 5-MS 8 are oriented to the $-x$-axis.

the Lagrangian function for Problem $\mathscr{P}_{2,\mathrm{c}}$ as

$$\mathcal{L} = \sum_{k=1}^{N_{\mathrm{MS}}} \zeta_k \log_2 \left(\frac{\sum_{j=1}^{N_{\mathrm{MS}}} g_{k,j} \, \bar{p}_j + a_k \, \bar{p}_k + P_{\mathrm{n}} \|\boldsymbol{w}_k\|^2}{\sum_{j=1,j\neq k}^{N_{\mathrm{MS}}} g_{k,j} \, \bar{p}_j + a_k \, \bar{p}_k + P_{\mathrm{n}} \|\boldsymbol{w}_k\|^2} \right)$$
$$+ \sum_{n=1}^{N_{\mathrm{BS}}} \mu_n \left(P_{\mathrm{t}} - \sum_{k=1}^{N_{\mathrm{MS}}} \|\boldsymbol{f}_{n,k}^{\mathrm{d}}\|^2 \, \bar{p}_k \right) \quad (49)$$

where μ_n is a Lagrangian multiplier. From the stationarity condition, i.e., $\frac{\partial \mathcal{L}}{\partial \bar{p}_k} = 0$ and primary feasibility, i.e., $\bar{p}_k \geq 0$ of the KKT conditions, we derive the following power update equation,

$$\bar{p}_k = \frac{1}{a_k + g_{k,k}} \left[\frac{(1 - \epsilon_k) \, g_{k,k} \, \zeta_k}{t_k + \log 2 \sum_{n=1}^{N_{\mathrm{BS}}} \mu_n \|\boldsymbol{f}_{n,k}^{\mathrm{d}}\|^2} - b_k \right]^+ \quad (50a)$$

for $k = 1, 2, \ldots, N_{\mathrm{MS}}$, where

$$b_k \triangleq \sum_{j=1,j\neq k}^{N_{\mathrm{MS}}} g_{k,j} \, \bar{p}_j + P_{\mathrm{n}} \|\boldsymbol{w}_k\|^2 \quad (50b)$$

$$\epsilon_k \triangleq \frac{a_k \, \bar{p}_k}{a_k \, \bar{p}_k + b_k} \quad (50c)$$

$$t_k \triangleq \sum_{m=1,m\neq k}^{N_{\mathrm{MS}}} \frac{\zeta_m \, \gamma_m \, g_{m,k}}{(g_{m,m} + a_m)\bar{p}_m + b_m} \, . \quad (50d)$$

In (50a), $[x]^+$ is defined as $[x]^+ \triangleq \max\{x, 0\}$.

Based on the above approach, we solve Problem $\mathscr{P}_{2,\mathrm{a}}$ by alternately updating the BF vectors and power scaling factors. Specifically, in each outer iteration, (45) is iteratively updated and then (50a) is updated for given $\bar{\boldsymbol{f}}_k, b_k, \epsilon_k, t_k$. In (50a), the values of μ_n should be determined to satisfy the power constraint in (48). This can be solved by the multi-dimensional bisection method because $\bar{p}_k$ is a monotonic function of μ_n. Note that the values of $\bar{p}_k$ in the right-hand side of (50a) are taken from that of the previous iteration. The proposed algorithm for joint baseband BF and power allocation of data transmission is summarized in Algorithm 2.

V. SIMULATION RESULTS

We now presents results for a case study where the BSs and MSs are located at fixed positions as in Fig. 2. The MSs can be thought of as cars or other IoT devices. We set $N_{\mathrm{BS}} = 6$ and $N_{\mathrm{MS}} = 8$ in most cases. The antenna arrays of the BSs and MSs are located at the heights of $15\,\mathrm{m}$ and of $1.5\,\mathrm{m}$, respectively.

Algorithm 2: Joint baseband BF and power allocation of data transmission

Require: $P_{\mathrm{t}}, \boldsymbol{P}_n^{\mathrm{p}}, \hat{\boldsymbol{F}}_n^{\mathrm{d}}, \boldsymbol{w}_k$, for $n = 1, 2, \ldots, N_{\mathrm{BS}}$, $k = 1, 2, \ldots, N_{\mathrm{MS}}$
1: $\bar{p}_k \leftarrow P_{\mathrm{t}}/N_{\mathrm{MS}}, \forall k$
2: $\bar{\boldsymbol{f}}_k \leftarrow \bar{\boldsymbol{h}}_{k,k}^\dagger / \|\mathrm{diag}(\hat{\boldsymbol{F}}_1^{\mathrm{d}}, \ldots, \hat{\boldsymbol{F}}_{N_{\mathrm{BS}}}^{\mathrm{d}})\bar{\boldsymbol{h}}_{k,k}\|, \forall k$
3: **while** $\bar{p}_k$ does not converge within max iteration **do**
4:      **while** $\bar{\boldsymbol{f}}_k, \forall k$ does not converge within max iteration **do**
5:          Update $\boldsymbol{A}_k$ and $\boldsymbol{B}_k$
6:          $\bar{\boldsymbol{f}}_k \leftarrow$ (45), $\forall k$
7:      **end while**
8:      **while** $\bar{p}_k$ does not converge within max iteration **do**
9:          Update b_k, ϵ_k, t_k from (50b), (50c), (50d)
10:         $(\mu_n^{(\mathrm{lo})}, \mu_n^{(\mathrm{up})}) \leftarrow (0, \mu_n^{(\max)}), \forall n$
11:         $\mu_n \leftarrow (\mu_n^{(\mathrm{lo})} + \mu_n^{(\mathrm{up})})/2, \forall n$
12:         **while** P_n^{sum} or μ_n does not converge **do**
13:             $\bar{p}_k \leftarrow$ (50a), $\forall k$
14:             $\mu_n \leftarrow (\mu_n^{(\mathrm{lo})} + \mu_n^{(\mathrm{up})})/2, \forall n$
15:             $P_n^{\mathrm{sum}} \leftarrow \sum_k \|\hat{\boldsymbol{F}}_n^{\mathrm{d}} \check{\boldsymbol{f}}_{n,k}^{\mathrm{d}}\|^2 \bar{p}_k, \forall n$
16:             **if** $P_n^{\mathrm{sum}} > P_{\mathrm{t}}$ **then**
17:                 $\mu_n^{(\mathrm{lo})} \leftarrow \mu_n, \forall n$
18:             **else**
19:                 $\mu_n^{(\mathrm{up})} \leftarrow \mu_n, \forall n$
20:             **end if**
21:         **end while**
22:     **end while**
23: **end while**
24: Obtain $\{\check{\boldsymbol{F}}_n^{\mathrm{d}}, \forall n\}$ from $\{\bar{\boldsymbol{f}}_k, \forall k\}$
25: Obtain $\{\boldsymbol{P}_n^{\mathrm{d}}, \forall n\}$ from $\{\bar{\boldsymbol{f}}_k, \bar{p}_k, \forall k\}$
Return: $\check{\boldsymbol{F}}_n^{\mathrm{d}}, \boldsymbol{P}_n^{\mathrm{d}}, \forall n$

The BSs use identical uniform planar arrays (UPAs) where N_{tx} is equal to the product of the numbers of antenna elements in x and z axes. The MSs use cylindrical arrays, which can be thought of as a product of a circular array and a linear array. The carrier frequency and the bandwidth are set to 38 GHz and 200 MHz, respectively. The channel coherence time is $T_{\mathrm{c}} = 0.1$ ms. The noise spectral density is assumed as -174 dBm/Hz. We use the path-loss model for mmWave channels presented in [91, Table A1-4]. The number of multi-path components is set as $L = 1$ to obtain useful insights in LOS-dominant mmWave channels. The noise figure at each MS is assumed as 8 dB. The position information and orientation information from the GNSS of the MSs are assumed to have random errors within 1 m radius in x-y plane and 10° in both angles, respectively. We use different values of P_{t}, N_{tx}, and N_{rx} in simulations. The performance of the proposed scheme is evaluated using Algorithm 1 and Algorithm 2, while the baseline schemes are compared by replacing one of the algorithms by the conventional algorithm.

Fig. 3 shows the contour plots of different performance metrics for various locations of a single MS within the network. Since $N_{\mathrm{MS}} = 1$, all the BSs have the same pilot power of P_{t}.

(a) Square root of SPEB [m]

(b) Square root of SOEB [deg]

(c) Achievable rate [Gbps]

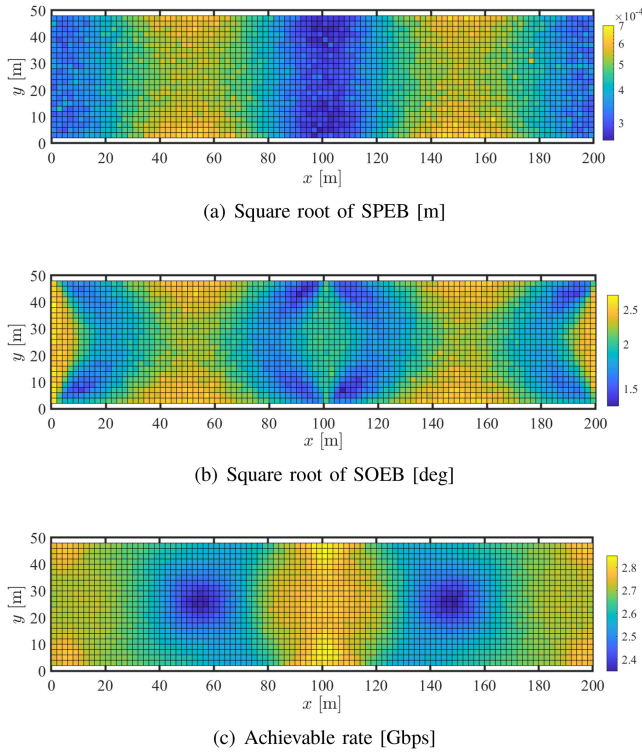Fig. 3. Contour plots for different metrics in the network: $N_{BS} = 6, N_{MS} = 1, N_{tx} = 10 \times 8, N_{rx} = 10 \times 4, P_t = 30$ dBm with fixed pilot length of $N_p = 667$.

The pilot length is fixed as $N_p = 667$ to observe the performance behaviors as a function of the MS locations. Interestingly, the performance behaviors of the three metrics have different tendencies along with the MS locations. For example, the position error is minimized when the MS is located between the two parallel BSs in y-axis, while the orientation error is minimized in diagonal directions from each BS. The achievable rate is maximized in front of each BS. These results indicate that the pilot length and pilot power should be jointly optimized particularly for multiple MSs to ensure uniformly-good performances.

Fig. 4 compares the trade-off between the achievable sum-rate and the maximum position error among the MSs for different P_t. It can be noticed that as the positioning accuracy improves, the achievable rate increases at first because the CSI estimation also improves. However, if a very accurate positioning is required, the achievable rate may decrease as the pilot length increases. Note also that only the right side of the point of the maximum sum rate is meaningful when comparing the rate-accuracy trade-off curves because the rates in the left side can also be achieved in the right side even with smaller positioning error bounds. Therefore, the improvement of the proposed scheme compared to the baseline schemes can be quantified by observing the line between the peak data rate in y-axis and the minimum localization error in x-axis. Observing the figure, the proposed scheme has a better rate-accuracy trade-off than that of the baseline schemes. We omit the trade-off curve between the rate and orientation error because it is similar to that of the positioning error.
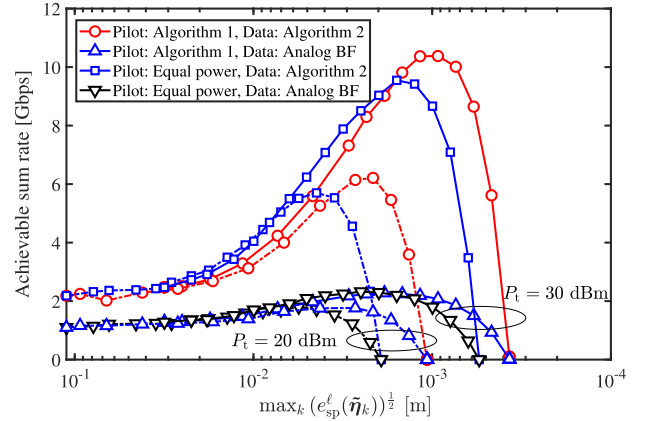
Fig. 4. Rate-accuracy region for different P_t: $N_{tx} = 10 \times 6$ and $N_{rx} = 10 \times 4$. The baseline curves are plotted by varying N_p with $\boldsymbol{P}_n^p = \frac{P_t}{N_{MS}} \boldsymbol{I}_{N_{MS}}, \forall n$.

Fig. 5(a) and Fig. 5(b) show the individual rate-accuracy region of the MSs for the baseline scheme and the proposed scheme, respectively. It can be noticed that the proposed scheme can provide similar localization performances with fairness for different MSs even in the presence of inaccurate GNSS information by setting the same accuracy constraint for the MSs. On the other hand, the baseline scheme provides different rate-accuracy region among the MSs in Fig. 5(a). Note that the average achievable rate for different MSs can also be evenly served by adjusting the weights ζ_k with the techniques in [85].

Fig. 6 verifies the asymptotic upper bound of the achievable rate in (39), which is used in the baseband BF design and power allocation. It is observed that the exact sum rate approaches to the approximated expression as N_{tx} or P_t increases.

Fig. 7 presents the effects of N_{tx} and N_{rx} on the rate-accuracy region. It can be observed that the use of a larger N_{tx} or a larger N_{rx} contributes to increase the maximum achievable sum rate and to reduce the minimum positioning error. In particular, increasing N_{rx} is more effective to improve the rate-accuracy region than increasing N_{tx}.

Fig. 8 shows convergence behaviors of the proposed algorithms for a channel realization. Fig. 8(a) shows the values of N_p within the procedure of the bisection search in Algorithm 1 for different requirements of localization accuracies. It is observed that a longer pilot length is required as the required accuracy increases. In addition, Fig. 8(b) shows that the values of $\bar{p}_k$ in Algorithm 2 converge within only a few iterations.

VI. CONCLUSION

This paper has proposed a cooperative BF and power allocation scheme for pilot and data transmissions with pilot length optimization in mmWave joint communication and localization systems. The user-centric design approach enables to balance the amount of channel usages between pilot and data transmissions and to uniformly provide the localization accuracy for the MSs by setting the same accuracy constraint. Particularly, the joint optimization of pilot length and power provides flexibility in the rate-accuracy region. Then design of the cooperative BF
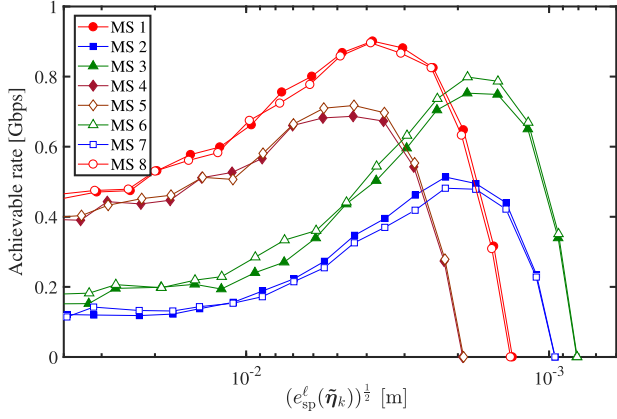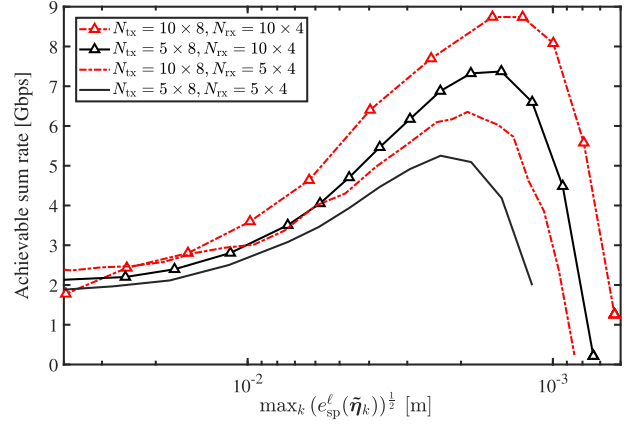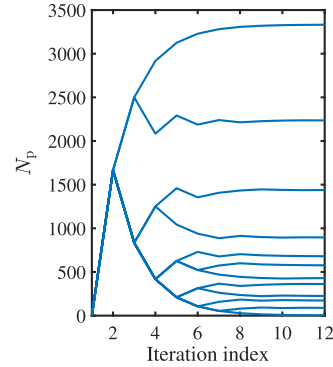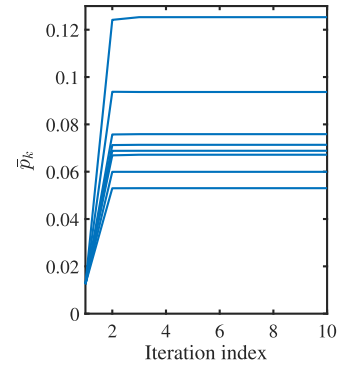
(a) Baseline scheme with equal pilot power allocation
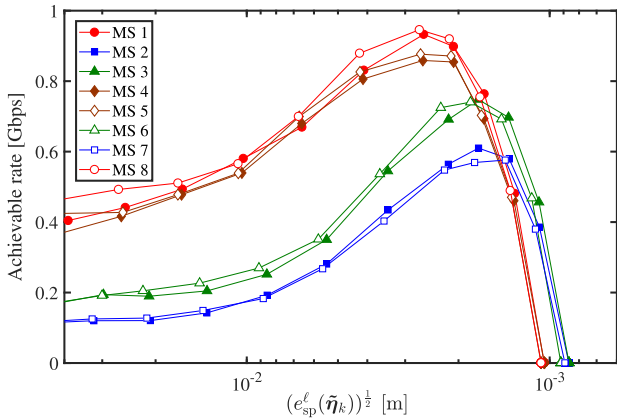
(b) Proposed scheme

Fig. 5. Individual rate-accuracy region of the MSs: $N_{\text{tx}} = 10 \times 6$, $N_{\text{rx}} = 10 \times 4$, and $P_{\text{t}} = 20$ dBm.
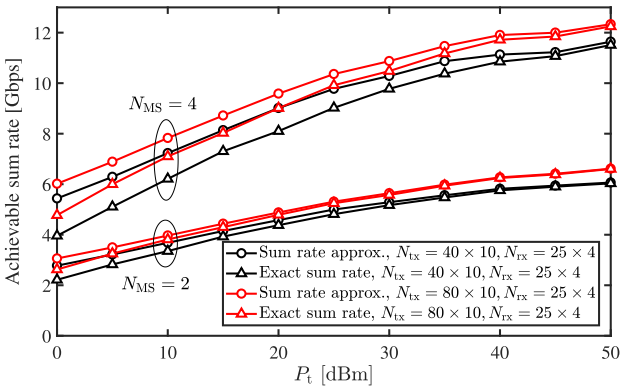
Fig. 6. Verification of asymptotic sum rate expression: $N_{\text{BS}} = 6$ with a fixed pilot length of $N_{\text{p}} = 1,000$.

Fig. 7. Rate-accuracy region of the proposed scheme for different N_{tx} and N_{rx}: $P_{\text{t}} = 25$ dBm.

(a) Algorithm 1   (b) Algorithm 2

Fig. 8. Convergence behaviors of the proposed algorithms: $N_{\text{tx}} = 10 \times 6$, $N_{\text{rx}} = 10 \times 4$, and $P_{\text{t}} = 20$ dBm.

that mmWave networks can efficiently support the users with different requirements of data rate and localization accuracy.

APPENDIX A
DERIVATION OF FIM IN (12)

Before deriving the elements of $\mathbf{J}_{\boldsymbol{\eta}_{n,k}}$, we define the short notations ignoring the indices n and k as follows,

$$\boldsymbol{a}_{\text{x},l} \triangleq \boldsymbol{a}_{\text{x}}(\varphi_{n,k,l}^{\text{x}}, \theta_{n,k,l}^{\text{x}}) \tag{51a}$$

$$\dot{\boldsymbol{a}}_{\text{x},\varphi,l} \triangleq \frac{\partial \boldsymbol{G}_{\text{x}}^{\text{T}} \boldsymbol{k}(\varphi_{n,k,l}^{\text{x}}, \theta_{n,k,l}^{\text{x}})}{\partial \varphi_{n,k,l}^{\text{x}}} \odot \boldsymbol{a}_{\text{x},l} \tag{51b}$$

$$\dot{\boldsymbol{a}}_{\text{x},\theta,l} \triangleq \frac{\partial \boldsymbol{G}_{\text{x}}^{\text{T}} \boldsymbol{k}(\varphi_{n,k,l}^{\text{x}}, \theta_{n,k,l}^{\text{x}})}{\partial \theta_{n,k,l}^{\text{x}}} \odot \boldsymbol{a}_{\text{x},l} \tag{51c}$$

$$\boldsymbol{G}_{\text{x}} \triangleq \left[\boldsymbol{g}_{\text{x},1}, \boldsymbol{g}_{\text{x},2}, \ldots, \boldsymbol{g}_{\text{x},N_{\text{x}}} \right] \in \mathbb{R}^{3 \times N_{\text{x}}} \tag{51d}$$

for $\text{x} \in \{\text{t}, \text{r}\}$. In (51d), $\boldsymbol{g}_{\text{x},m}$ is the relative position vector of the mth antenna element with the origin at the array center. Using the definitions in (A), the elements of $\mathbf{J}_{\boldsymbol{\eta}_{n,k}}$ are derived as follows,

$$\mathsf{J}_{\varphi_{n,k,l}^{\text{r}}, \varphi_{n,k,l'}^{\text{r}}} = \gamma_{\text{p}} \Re \left\{ \left(\alpha_l^* \alpha_{l'} \dot{\boldsymbol{a}}_{\text{r},\varphi,l}^\dagger \dot{\boldsymbol{a}}_{\text{r},\varphi,l'} \right) \left(\boldsymbol{a}_{\text{t},l'}^\dagger \boldsymbol{V}_n \boldsymbol{a}_{\text{t},l} \right) R_{l,l'}^{(0)} \right\}$$

and power allocation for data transmission is made possible by taking into account the imperfect estimation and using all the remaining time resources. It is shown that the proposed scheme can improve significantly the rate-accuracy region by efficiently exploiting the wireless resources. From the results, we conclude

$$\mathsf{J}_{\varphi^{r}_{n,k,l},\theta^{r}_{n,k,l'}} = \gamma_{p}\Re\{(\alpha^{*}_{l}\alpha_{l'}\dot{a}^{\dagger}_{r,\varphi,l}\dot{a}_{r,\theta,l'})(a^{\dagger}_{t,l'}V_{n}a_{t,l})R^{(0)}_{l,l'}\}$$

$$\mathsf{J}_{\varphi^{r}_{n,k,l},\varphi^{t}_{n,k,l'}} = -\gamma_{p}\Re\{(\alpha^{*}_{l}\alpha_{l'}\dot{a}^{\dagger}_{r,\varphi,l}a_{r,l'})(\dot{a}^{\dagger}_{t,\varphi,l'}V_{n}a_{t,l})R^{(0)}_{l,l'}\}$$

$$\mathsf{J}_{\varphi^{r}_{n,k,l},\theta^{t}_{n,k,l'}} = -\gamma_{p}\Re\{(\alpha^{*}_{l}\alpha_{l'}\dot{a}^{\dagger}_{r,\varphi,l}a_{r,l'})(\dot{a}^{\dagger}_{t,\theta,l'}V_{n}a_{t,l})R^{(0)}_{l,l'}\}$$

$$\mathsf{J}_{\varphi^{r}_{n,k,l},\tau_{n,k,l'}} = \gamma_{p}\Re\{j(\alpha^{*}_{l}\alpha_{l'}\dot{a}^{\dagger}_{r,\varphi,l}a_{r,l'})(a^{\dagger}_{t,l'}V_{n}a_{t,l})R^{(1)}_{l,l'}\}$$

$$\mathsf{J}_{\varphi^{r}_{n,k,l},\alpha^{(R)}_{n,k,l'}} = \gamma_{p}\Re\{j(\alpha^{*}_{l}\dot{a}^{\dagger}_{r,\varphi,l}a_{r,l'})(a^{\dagger}_{t,l'}V_{n}a_{t,l})R^{(0)}_{l,l'}\}$$

$$\mathsf{J}_{\varphi^{r}_{n,k,l},\alpha^{(I)}_{n,k,l'}} = -\gamma_{p}\Re\{(\alpha^{*}_{l}\dot{a}^{\dagger}_{r,\varphi,l}a_{r,l'})(a^{\dagger}_{t,l'}V_{n}a_{t,l})R^{(0)}_{l,l'}\}$$

$$\mathsf{J}_{\theta^{r}_{n,k,l},\theta^{r}_{n,k,l'}} = \gamma_{p}\Re\{(\alpha^{*}_{l}\alpha_{l'}\dot{a}^{\dagger}_{r,\theta,l}\dot{a}_{r,\theta,l'})(a^{\dagger}_{t,l'}V_{n}a_{t,l})R^{(0)}_{l,l'}\}$$

$$\mathsf{J}_{\theta^{r}_{n,k,l},\varphi^{t}_{n,k,l'}} = -\gamma_{p}\Re\{(\alpha^{*}_{l}\alpha_{l'}\dot{a}^{\dagger}_{r,\theta,l}a_{r,l'})(\dot{a}^{\dagger}_{t,\varphi,l'}V_{n}a_{t,l})R^{(0)}_{l,l'}\}$$

$$\mathsf{J}_{\theta^{r}_{n,k,l},\theta^{t}_{n,k,l'}} = -\gamma_{p}\Re\{(\alpha^{*}_{l}\alpha_{l'}\dot{a}^{\dagger}_{r,\theta,l}a_{r,l'})(\dot{a}^{\dagger}_{t,\theta,l'}V_{n}a_{t,l})R^{(0)}_{l,l'}\}$$

$$\mathsf{J}_{\theta^{r}_{n,k,l},\tau_{n,k,l'}} = \gamma_{p}\Re\{j(\alpha^{*}_{l}\alpha_{l'}\dot{a}^{\dagger}_{r,\theta,l}a_{r,l'})(a^{\dagger}_{t,l'}V_{n}a_{t,l})R^{(1)}_{l,l'}\}$$

$$\mathsf{J}_{\theta^{r}_{n,k,l},\alpha^{(R)}_{n,k,l'}} = \gamma_{p}\Re\{j(\alpha^{*}_{l}\dot{a}^{\dagger}_{r,\theta,l}a_{r,l'})(a^{\dagger}_{t,l'}V_{n}a_{t,l})R^{(0)}_{l,l'}\}$$

$$\mathsf{J}_{\theta^{r}_{n,k,l},\alpha^{(I)}_{n,k,l'}} = -\gamma_{p}\Re\{(\alpha^{*}_{l}\dot{a}^{\dagger}_{r,\theta,l}a_{r,l'})(a^{\dagger}_{t,l'}V_{n}a_{t,l})R^{(0)}_{l,l'}\}$$

$$\mathsf{J}_{\varphi^{t}_{n,k,l},\varphi^{t}_{n,k,l'}} = \gamma_{p}\Re\{(\alpha^{*}_{l}\alpha_{l'}a^{\dagger}_{r,l}a_{r,l'})(\dot{a}^{\dagger}_{t,\varphi,l'}V_{n}\dot{a}_{t,\varphi,l})R^{(0)}_{l,l'}\}$$

$$\mathsf{J}_{\varphi^{t}_{n,k,l},\theta^{t}_{n,k,l'}} = \gamma_{p}\Re\{(\alpha^{*}_{l}\alpha_{l'}a^{\dagger}_{r,l}a_{r,l'})(\dot{a}^{\dagger}_{t,\theta,l'}V_{n}\dot{a}_{t,\varphi,l})R^{(0)}_{l,l'}\}$$

$$\mathsf{J}_{\varphi^{t}_{n,k,l},\tau_{n,k,l'}} = -\gamma_{p}\Re\{j(\alpha^{*}_{l}\alpha_{l'}a^{\dagger}_{r,l}a_{r,l'})(a^{\dagger}_{t,l'}V_{n}\dot{a}_{t,\varphi,l})R^{(1)}_{l,l'}\}$$

$$\mathsf{J}_{\varphi^{t}_{n,k,l},\alpha^{(R)}_{n,k,l'}} = -\gamma_{p}\Re\{j(\alpha^{*}_{l}a^{\dagger}_{r,l}a_{r,l'})(a^{\dagger}_{t,l'}V_{n}\dot{a}_{t,\varphi,l})R^{(0)}_{l,l'}\}$$

$$\mathsf{J}_{\varphi^{t}_{n,k,l},\alpha^{(I)}_{n,k,l'}} = \gamma_{p}\Re\{(\alpha^{*}_{l}a^{\dagger}_{r,l}a_{r,l'})(a^{\dagger}_{t,l'}V_{n}\dot{a}_{t,\varphi,l})R^{(0)}_{l,l'}\}$$

$$\mathsf{J}_{\theta^{t}_{n,k,l},\theta^{t}_{n,k,l'}} = \gamma_{p}\Re\{(\alpha^{*}_{l}\alpha_{l'}a^{\dagger}_{r,l}a_{r,l'})(\dot{a}^{\dagger}_{t,\theta,l'}V_{n}\dot{a}_{t,\theta,l})R^{(0)}_{l,l'}\}$$

$$\mathsf{J}_{\theta^{t}_{n,k,l},\tau_{n,k,l'}} = -\gamma_{p}\Re\{j(\alpha^{*}_{l}\alpha_{l'}a^{\dagger}_{r,l}a_{r,l'})(a^{\dagger}_{t,l'}V_{n}\dot{a}_{t,\theta,l})R^{(1)}_{l,l'}\}$$

$$\mathsf{J}_{\theta^{t}_{n,k,l},\alpha^{(R)}_{n,k,l'}} = -\gamma_{p}\Re\{j(\alpha^{*}_{l}a^{\dagger}_{r,l}a_{r,l'})(a^{\dagger}_{t,l'}V_{n}\dot{a}_{t,\theta,l})R^{(0)}_{l,l'}\}$$

$$\mathsf{J}_{\theta^{t}_{n,k,l},\alpha^{(I)}_{n,k,l'}} = \gamma_{p}\Re\{(\alpha^{*}_{l}a^{\dagger}_{r,l}a_{r,l'})(a^{\dagger}_{t,l'}V_{n}\dot{a}_{t,\theta,l})R^{(0)}_{l,l'}\}$$

$$\mathsf{J}_{\tau_{n,k,l},\tau_{n,k,l'}} = \gamma_{p}\Re\{(\alpha^{*}_{l}\alpha_{l'}a^{\dagger}_{r,l}a_{r,l'})(a^{\dagger}_{t,l'}V_{n}a_{t,l})R^{(2)}_{l,l'}\}$$

$$\mathsf{J}_{\tau_{n,k,l},\alpha^{(R)}_{n,k,l'}} = \gamma_{p}\Re\{(\alpha^{*}_{l}a^{\dagger}_{r,l}a_{r,l'})(a^{\dagger}_{t,l'}V_{n}a_{t,l})R^{(1)}_{l,l'}\}$$

$$\mathsf{J}_{\tau_{n,k,l},\alpha^{(I)}_{n,k,l'}} = \gamma_{p}\Re\{j(\alpha^{*}_{l}a^{\dagger}_{r,l}a_{r,l'})(a^{\dagger}_{t,l'}V_{n}a_{t,l})R^{(1)}_{l,l'}\}$$

$$\mathsf{J}_{\alpha^{(R)}_{n,k,l},\alpha^{(R)}_{n,k,l'}} = \gamma_{p}\Re\{(a^{\dagger}_{r,l}a_{r,l'})(a^{\dagger}_{t,l'}V_{n}a_{t,l})R^{(0)}_{l,l'}\}$$

$$\mathsf{J}_{\alpha^{(R)}_{n,k,l},\alpha^{(I)}_{n,k,l'}} = \gamma_{p}\Re\{j(a^{\dagger}_{r,l}a_{r,l'})(a^{\dagger}_{t,l'}V_{n}a_{t,l})R^{(0)}_{l,l'}\}$$

$$\mathsf{J}_{\alpha^{(I)}_{n,k,l},\alpha^{(I)}_{n,k,l'}} = \gamma_{p}\Re\{(a^{\dagger}_{r,l}a_{r,l'})(a^{\dagger}_{t,l'}V_{n}a_{t,l})R^{(0)}_{l,l'}\}$$

where

$$\gamma_{p} \triangleq \frac{N_{rx}N_{tx}N_{p}}{P_{n}}$$

$$V_{n} \triangleq F^{p}_{n}(P^{p}_{n})^{\frac{1}{2}}\mathbf{1}_{N_{MS}\times N_{MS}}(P^{p}_{n})^{\frac{1}{2}}(F^{p}_{n})^{\dagger}.$$

Also, ignoring the indices n and k, the cross correlations are defined as

$$R^{(0)}_{l,l'} \triangleq \int_{0}^{N_{p}T_{s}}(s^{p}_{n}(t-\tau_{n,k,l}))^{*}s^{p}_{n}(t-\tau_{n,k,l'})\,dt \quad (52a)$$

$$R^{(1)}_{l,l'} \triangleq \int_{0}^{N_{p}T_{s}}(s^{p}_{n}(t-\tau_{n,k,l}))^{*}\frac{\partial s^{p}_{n}(t-\tau_{n,k,l'})}{\partial\tau_{n,k,l'}}\,dt \quad (52b)$$

$$R^{(2)}_{l,l'} \triangleq \int_{0}^{N_{p}T_{s}}\frac{\partial(s^{p}_{n}(t-\tau_{n,k,l}))^{*}}{\partial\tau_{n}}\frac{\partial s^{p}_{n}(t-\tau_{n,k,l'})}{\partial\tau_{n,k,l'}}\,dt \quad (52c)$$

where using the Parseval's theorem, (52) leads to

$$R^{(i)}_{l,l'} = \int_{-B/2}^{B/2}(2\pi f)^{i}|P(f)|^{2}\exp(-j2\pi f(\tau_{n,k,l'}-\tau_{n,k,l}))\,df. \quad (53)$$

Since $R^{(1)}_{l,l} = 0$ in (53), the values of $\mathsf{J}_{\varphi^{r}_{l},\tau_{l}}$, $\mathsf{J}_{\theta^{r}_{l},\tau_{l}}$, $\mathsf{J}_{\varphi^{t}_{l},\tau_{l}}$, $\mathsf{J}_{\theta^{t}_{l},\tau_{l}}$, $\mathsf{J}_{\tau_{l},\alpha^{(R)}_{l}}$, and $\mathsf{J}_{\tau_{l},\alpha^{(I)}_{l}}$ are always zero. Also, $R^{(i)}_{l,l'} = 0$ if $l \neq l'$.

APPENDIX B
APPROXIMATED BLOCK-DIAGONAL SUBMATRIX IN (14)

In (14), each submatrix is approximated by a block-diagonal structure when F^{p}_{n} includes array steering vectors with large N_{tx}. The entries of $\mathbf{J}_{\eta_{n,k,l}}$ are given as

$$[\mathbf{J}_{\eta_{n,k,l}}]_{1:2,1:2} = \begin{bmatrix} \mathsf{J}_{\varphi^{r}_{n,k,l},\varphi^{r}_{n,k,l}} & \mathsf{J}_{\varphi^{r}_{n,k,l},\theta^{r}_{n,k,l}} \\ \mathsf{J}_{\theta^{r}_{n,k,l},\varphi^{r}_{n,k,l}} & \mathsf{J}_{\theta^{r}_{n,k,l},\theta^{r}_{n,k,l}} \end{bmatrix} \quad (54a)$$

$$[\mathbf{J}_{\eta_{n,k,l}}]_{3:4,3:4} = \begin{bmatrix} \mathsf{J}_{\varphi^{t}_{n,k,l},\varphi^{t}_{n,k,l}} & \mathsf{J}_{\varphi^{t}_{n,k,l},\theta^{t}_{n,k,l}} \\ \mathsf{J}_{\theta^{t}_{n,k,l},\varphi^{t}_{n,k,l}} & \mathsf{J}_{\theta^{t}_{n,k,l},\theta^{t}_{n,k,l}} \end{bmatrix} \quad (54b)$$

$$[\mathbf{J}_{\eta_{n,k,l}}]_{5,5} = \mathsf{J}_{\tau_{n,k,l},\tau_{n,k,l}} \quad (54c)$$

$$[\mathbf{J}_{\eta_{n,k,l}}]_{6,6} = \mathsf{J}_{\alpha^{(R)}_{n,k,l},\alpha^{(R)}_{n,k,l}} \quad (54d)$$

$$[\mathbf{J}_{\eta_{n,k,l}}]_{7,7} = \mathsf{J}_{\alpha^{(I)}_{n,k,l},\alpha^{(I)}_{n,k,l}} \quad (54e)$$

where the elements of $\eta_{n,k,l}$ can be found in (10).

APPENDIX C
PROOF FOR THE APPROXIMATION IN (54)

For large N_{rx}, N_{tx}, and B, the following asymptotic results hold,

$$\lim_{N_{x}\to\infty}A^{\dagger}_{x}A_{x} = I \quad (55)$$

$$\lim_{N_{x}\to\infty}\dot{A}^{\dagger}_{x,\varphi}A_{x} = \lim_{N_{x}\to\infty}\dot{A}^{\dagger}_{x,\theta}A_{x} = \mathbf{0} \quad (56)$$

where the definitions of A_{x}, $\dot{A}_{x,\varphi}$, $\dot{A}_{x,\theta}$ are given by using (51) as

$$A_{x} \triangleq [a_{x,1}, a_{x,2}, \ldots, a_{x,L}] \quad (57a)$$

$$\dot{\boldsymbol{A}}_{\mathrm{x},\varphi} \triangleq [\dot{\boldsymbol{a}}_{\mathrm{x},\varphi,1}, \dot{\boldsymbol{a}}_{\mathrm{x},\varphi,2}, \ldots, \dot{\boldsymbol{a}}_{\mathrm{x},\varphi,L}] \tag{57b}$$

$$\dot{\boldsymbol{A}}_{\mathrm{x},\theta} \triangleq [\dot{\boldsymbol{a}}_{\mathrm{x},\theta,1}, \dot{\boldsymbol{a}}_{\mathrm{x},\theta,2}, \ldots, \dot{\boldsymbol{a}}_{\mathrm{x},\theta,L}]. \tag{57c}$$

The proofs for (55) and (56) can be found in [83, eq. (65)] and [28, eq. (18)], respectively. Also, from [28, eq. (21) and eq. (22)], the cross correlation terms defined in (52a) and (52b) satisfy the following limits

$$\lim_{B \to \infty} R_{l,l'}^{(0)} = 0, \text{ for } l \neq l' \tag{58}$$

$$\lim_{B \to \infty} R_{l,l'}^{(1)} = 0, \forall l, l'. \tag{59}$$

APPENDIX D
DERIVATION OF THE MATRIX ELEMENTS IN (19)

Following the two-step transformation procedure in [28], we derive the elements of the matrix $\mathbf{T}_{n,k}$ in (19). First of all, we define the rotated position vectors

$$\boldsymbol{q}'_{n,k} \triangleq \boldsymbol{K}^{-1}(\phi_k^{\mathrm{r}}, \theta_k^{\mathrm{r}})(\boldsymbol{q}_n - \boldsymbol{p}_k) = [q'_{n,k,\mathrm{x}}, q'_{n,k,\mathrm{y}}, q'_{n,k,\mathrm{z}}]^{\mathrm{T}}$$

$$\boldsymbol{p}'_{n,k} \triangleq \boldsymbol{K}^{-1}(\phi_n^{\mathrm{t}}, \theta_n^{\mathrm{t}})(\boldsymbol{p}_k - \boldsymbol{q}_n) = [p'_{n,k,\mathrm{x}}, p'_{n,k,\mathrm{y}}, p'_{n,k,\mathrm{z}}]^{\mathrm{T}}$$

with the rotation matrix

$$\boldsymbol{K}(\phi, \theta) \triangleq \begin{bmatrix} \cos\phi & -\sin\phi\cos\theta & -\sin\phi\sin\theta \\ \sin\phi & \cos\phi\cos\theta & \cos\phi\sin\theta \\ 0 & -\sin\theta & \cos\theta \end{bmatrix}$$

where the column vectors are defined as $\boldsymbol{K}(\phi, \theta) = [\boldsymbol{k}_1 | \boldsymbol{k}_2 | \boldsymbol{k}_3]$. Then the AoAs for the LOS paths can be calculated as

$$\varphi_{n,k,1}^{\mathrm{r}} = \tan^{-1}\left(\frac{q'_{n,k,\mathrm{y}}}{q'_{n,k,\mathrm{x}}}\right)$$

$$\theta_{n,k,1}^{\mathrm{r}} = \cos^{-1}\left(\frac{q'_{n,k,\mathrm{z}}}{\|\boldsymbol{q}'_{n,k}\|}\right)$$

$$\tau_{n,k,1} = \frac{\|\boldsymbol{q}'_{n,k}\|}{c}$$

where c is the speed of light. The AoDs for the LOS paths can also be obtained as

$$\varphi_{n,k,1}^{\mathrm{t}} = \tan^{-1}\left(\frac{p'_{n,k,\mathrm{y}}}{p'_{n,k,\mathrm{x}}}\right) \text{ and } \theta_{n,k,1}^{\mathrm{t}} = \cos^{-1}\left(\frac{p'_{n,k,\mathrm{z}}}{\|\boldsymbol{p}'_{n,k}\|}\right).$$

Note that the calculations for the NLOS paths corresponding to $\tilde{\mathbf{p}}_{n,k,l}$ are omitted due to the similarity. From the above relationships, the following derivatives can be calculated,

$$\frac{\partial \varphi_{n,k,1}^{\mathrm{r}}}{\partial \boldsymbol{p}_k} = \frac{(\boldsymbol{k}_1 \boldsymbol{k}_2^{\mathrm{T}} - \boldsymbol{k}_2 \boldsymbol{k}_1^{\mathrm{T}})(\boldsymbol{q}_n - \boldsymbol{p}_k)}{(q'_{n,k,\mathrm{x}})^2 + (q'_{n,k,\mathrm{y}})^2}$$

$$\frac{\partial \theta_{n,k,1}^{\mathrm{r}}}{\partial \boldsymbol{p}_k} = \frac{1}{\sqrt{(q'_{n,k,\mathrm{x}})^2 + (q'_{n,k,\mathrm{y}})^2}}\left(\boldsymbol{k}_3 + \frac{q'_{n,k,\mathrm{z}}}{\|\boldsymbol{q}'_{n,k}\|^2}(\boldsymbol{p}_k - \boldsymbol{q}_n)\right)$$

$$\frac{\partial \varphi_{n,k,1}^{\mathrm{t}}}{\partial \boldsymbol{p}_k} = \frac{p'_{n,k,\mathrm{x}} \boldsymbol{k}_2 - p'_{n,k,\mathrm{y}} \boldsymbol{k}_1}{(p'_{n,k,\mathrm{x}})^2 + (p'_{n,k,\mathrm{y}})^2}$$

$$\frac{\partial \theta_{n,k,1}^{\mathrm{t}}}{\partial \boldsymbol{p}_k} = \frac{1}{\sqrt{(p'_{n,k,\mathrm{x}})^2 + (p'_{n,k,\mathrm{y}})^2}}\left(\frac{p'_{n,k,\mathrm{z}}}{\|\boldsymbol{p}'_{n,k}\|^2}(\boldsymbol{p}_k - \boldsymbol{q}_n) - \boldsymbol{k}_3\right)$$

$$\frac{\partial \tau_{n,k,1}}{\partial \boldsymbol{p}_k} = \frac{1}{c}\frac{\boldsymbol{p}_k - \boldsymbol{q}_n}{\|\boldsymbol{q}'_{n,k}\|}$$

$$\frac{\partial \varphi_{n,k,1}^{\mathrm{r}}}{\partial \phi_k^{\mathrm{r}}} = \frac{1}{\sqrt{(q'_{n,k,\mathrm{x}})^2 + (q'_{n,k,\mathrm{y}})^2}} \\ \times \begin{bmatrix} -q'_{n,k,\mathrm{x}}\cos\phi_k^{\mathrm{r}}\cos\theta_k^{\mathrm{r}} + q'_{n,k,\mathrm{y}}\sin\phi_k^{\mathrm{r}} \\ -q'_{n,k,\mathrm{x}}\sin\phi_k^{\mathrm{r}}\cos\theta_k^{\mathrm{r}} - q'_{n,k,\mathrm{y}}\cos\phi_k^{\mathrm{r}} \\ 0 \end{bmatrix}^{\mathrm{T}}(\boldsymbol{q}_n - \boldsymbol{p}_k)$$

$$\frac{\partial \varphi_{n,k,1}^{\mathrm{r}}}{\partial \theta_k^{\mathrm{r}}} = \frac{q'_{n,k,\mathrm{x}}}{\sqrt{(q'_{n,k,\mathrm{x}})^2 + (q'_{n,k,\mathrm{y}})^2}} \begin{bmatrix} \sin\phi_k^{\mathrm{r}}\sin\theta_k^{\mathrm{r}} \\ -\cos\phi_k^{\mathrm{r}}\sin\theta_k^{\mathrm{r}} \\ -\cos\theta_k^{\mathrm{r}} \end{bmatrix}^{\mathrm{T}}(\boldsymbol{q}_n - \boldsymbol{p}_k)$$

$$\frac{\partial \theta_{n,k,1}^{\mathrm{r}}}{\partial \phi_k^{\mathrm{r}}} = \frac{1}{\sqrt{(q'_{n,k,\mathrm{x}})^2 + (q'_{n,k,\mathrm{y}})^2}} \begin{bmatrix} -\cos\phi_k^{\mathrm{r}}\sin\theta_k^{\mathrm{r}} \\ -\sin\phi_k^{\mathrm{r}}\sin\theta_k^{\mathrm{r}} \\ 0 \end{bmatrix}^{\mathrm{T}}(\boldsymbol{p}_k - \boldsymbol{q}_n)$$

$$\frac{\partial \theta_{n,k,1}^{\mathrm{r}}}{\partial \theta_k^{\mathrm{r}}} = \frac{1}{\sqrt{(q'_{n,k,\mathrm{x}})^2 + (q'_{n,k,\mathrm{y}})^2}} \begin{bmatrix} -\sin\phi_k^{\mathrm{r}}\cos\theta_k^{\mathrm{r}} \\ \cos\phi_k^{\mathrm{r}}\cos\theta_k^{\mathrm{r}} \\ -\sin\theta_k^{\mathrm{r}} \end{bmatrix}^{\mathrm{T}}(\boldsymbol{p}_k - \boldsymbol{q}_n).$$

Note that the AoDs and delays are independent of orientation angles. The elements in $\mathbf{T}_{n,k}$ for NLOS paths can also be calculated with respect to $\tilde{\mathbf{p}}_k$ in the same way.

APPENDIX E
PROOF FOR THE APPROXIMATION IN (39)

Defining

$$\mathsf{x}_j \triangleq \sum_{n=1}^{N_{\mathrm{BS}}} \sum_{l=1}^{L} \sqrt{p_{n,j}^{\mathrm{d}}} \left(\mathbf{w}_k^{\mathrm{d}}\right)^{\dagger} \mathbf{E}_{n,k,l} \mathbf{f}_{n,j}^{\mathrm{d}}$$

the expectation term in (26) can be expressed by $\mathbb{E}\{|\sum_{n=1}^{N_{\mathrm{BS}}} \sum_{l=1}^{L} \sqrt{p_{n,j}^{\mathrm{d}}}(\mathbf{w}_k^{\mathrm{d}})^{\dagger}\mathbf{E}_{n,k,l}\mathbf{f}_{n,j}^{\mathrm{d}}|^2\} = \mathbb{E}\{|\mathsf{x}_j|^2\}$. Substituting $\mathbf{f}_{n,k}^{\mathrm{d}} = \hat{\mathbf{F}}_n^{\mathrm{d}}\check{\mathbf{f}}_{n,k}^{\mathrm{d}}$ from (37) and $\mathbf{w}_k^{\mathrm{d}} = \sum_{n=1}^{N_{\mathrm{BS}}} \boldsymbol{a}_{\mathrm{r}}(\hat{\varphi}_{n,k,1}^{\mathrm{r}}, \hat{\theta}_{n,k,1}^{\mathrm{r}})$ from (38) into x_j, we have

$$\mathsf{x}_j = \sum_{n=1}^{N_{\mathrm{BS}}} \sqrt{p_{n,j}^{\mathrm{d}}}\sqrt{N_{\mathrm{tx}}N_{\mathrm{rx}}}\left(\sum_{l=1}^{L} \hat{\alpha}_{n,k,l}\mathsf{B}_{\mathrm{r}}(n,k,l,k)\mathsf{B}_{\mathrm{t}}(n,k,l,j) \right. \\ \left. - \sum_{l=1}^{L} \alpha_{n,k,l}\mathsf{B}_{\mathrm{r}}(n,k,l,k)\mathsf{b}_{n,k,l,j}^{\mathrm{t}}\right)$$

where the beam pattern functions are defined as

$$\mathsf{B}_{\mathrm{r}}(n,k,l,i) \triangleq \boldsymbol{a}_{\mathrm{r}}^{\dagger}(\hat{\varphi}_{n,k,l}^{\mathrm{r}}, \hat{\theta}_{n,k,l}^{\mathrm{r}})\,\boldsymbol{a}_{\mathrm{t}}(\hat{\varphi}_{n,i,1}^{\mathrm{r}}, \hat{\theta}_{n,i,1}^{\mathrm{r}})$$

$$\mathsf{B}_{\mathrm{t}}(n,k,l,i) \triangleq \boldsymbol{a}_{\mathrm{t}}^{\dagger}(\varphi_{n,k,l}^{\mathrm{t}}, \theta_{n,k,l}^{\mathrm{t}})\,\boldsymbol{a}_{\mathrm{t}}(\hat{\varphi}_{n,i,1}^{\mathrm{t}}, \hat{\theta}_{n,i,1}^{\mathrm{t}})$$

$$\mathsf{b}_{n,k,l,j}^{\mathrm{t}} \triangleq \sum_{i=1}^{N_{\mathrm{MS}}} \mathsf{B}_{\mathrm{t}}(n,k,l,i)\left[\check{\mathbf{f}}_{n,j}^{\mathrm{d}}\right]_i$$

for $n = 1, 2, \ldots, N_{\mathrm{BS}}$ and $k, j = 1, 2, \ldots, N_{\mathrm{MS}}$. If N_{tx} and N_{rx} are large enough and the GNSS information is perfect, the functions $\mathsf{B}_{\mathrm{r}}(n,k,l,i)$ and $\mathsf{B}_{\mathrm{t}}(n,k,l,i)$ goes to 1 only if $k = i$

and $l = 1$ and 0 otherwise. Therefore, we have

$$|\mathsf{x}_j|^2 \to \sum_{n=1}^{N_{\mathrm{BS}}} p_{n,j}^{\mathrm{d}} \, N_{\mathrm{tx}} N_{\mathrm{rx}}$$
$$\times \underbrace{\left(|\widehat{\alpha}_{n,k,1}|^2 + |\alpha_{n,k,1}|^2 - \widehat{\alpha}_{n,k,1} \alpha_{n,k,1}^* - \alpha_{n,k,1} \widehat{\alpha}_{n,k,1}^* \right)}_{\text{(a)}}$$

for $j = k$, and $|\mathsf{x}_j|^2 \to 0$ for $j \neq k$. Using the fact that $x + x^* = 2\Re\{x\}$ and $\Re\{xy^*\} = \Re\{x\}\Re\{y\} + \Im\{x\}\Im\{y\}$, The expression (a) can be written as

$$(\text{a}) = |\widehat{\alpha}_{n,k,1}^{(\mathrm{R})}|^2 + |\widehat{\alpha}_{n,k,1}^{(\mathrm{I})}|^2 + |\alpha_{n,k,1}^{(\mathrm{R})}|^2 + |\alpha_{n,k,1}^{(\mathrm{I})}|^2$$
$$- 2\widehat{\alpha}_{n,k,1}^{(\mathrm{R})} \alpha_{n,k,1}^{(\mathrm{R})} - 2\widehat{\alpha}_{n,k,1}^{(\mathrm{I})} \alpha_{n,k,1}^{(\mathrm{I})} .$$

Since $\mathbb{E}\{(\alpha_{n,k,1}^{(\mathrm{R})} - \widehat{\alpha}_{n,k,1}^{(\mathrm{R})})^2\} \geqslant \mathrm{C}(\widehat{\alpha}_{n,k,1}^{(\mathrm{R})})$ for unbiased and efficient estimators, $\mathbb{E}\{|\mathsf{x}_k|^2\}$ can be asymptotically lower bounded by

$$\mathbb{E}\left\{|\mathsf{x}_k|^2\right\} \gtrsim \sum_{n=1}^{N_{\mathrm{BS}}} p_{n,j}^{\mathrm{d}} N_{\mathrm{tx}} N_{\mathrm{rx}} \left(\mathrm{C}(\widehat{\alpha}_{n,k,1}^{(\mathrm{R})}) + \mathrm{C}(\widehat{\alpha}_{n,k,1}^{(\mathrm{I})}) \right) .$$

Applying similar analysis of using the beam pattern functions to (15f), we have $\mathrm{C}(\widehat{\alpha}_{n,k,1}^{(\mathrm{R})}) = \mathrm{C}(\widehat{\alpha}_{n,k,1}^{(\mathrm{I})}) = 1/(\gamma_{\mathrm{p}} p_{n,k}^{\mathrm{p}})$. From this, we obtain

$$\mathbb{E}\left\{|\mathsf{x}_k|^2\right\} \gtrsim \frac{2P_{\mathrm{n}}}{N_{\mathrm{p}}} \sum_{n=1}^{N_{\mathrm{BS}}} \frac{p_{n,k}^{\mathrm{d}}}{p_{n,k}^{\mathrm{p}}} \quad \text{and} \quad \mathbb{E}\left\{|\mathsf{x}_j|^2\right\} \to 0, j \neq k$$

as $N_{\mathrm{tx}} \to \infty$ and $N_{\mathrm{rx}} \to \infty$, which leads to (39).

REFERENCES

[1] J. Choi, V. Va, N. Gonzalez-Prelcic, R. Daniels, C. R. Bhat, and R. W. Heath, "Millimeter-wave vehicular communication to support massive automotive sensing," *IEEE Commun. Mag.*, vol. 54, no. 12, pp. 160–167, Dec. 2016.

[2] W. Saad, M. Bennis, and M. Chen, "A vision of 6 G wireless systems: Applications, trends, technologies, and open research problems," *IEEE Netw.*, vol. 34, no. 3, pp. 134–142, May/Jun. 2020.

[3] M. Z. Win *et al.*, "Network localization and navigation via cooperation," *IEEE Commun. Mag.*, vol. 49, no. 5, pp. 56–62, May 2011.

[4] G. Bresson, Z. Alsayed, L. Yu, and S. Glaser, "Simultaneous localization and mapping: A survey of current trends in autonomous driving," *IEEE Trans. Intell. Transp. Syst.*, vol. 2, no. 3, pp. 194–220, Sep. 2017.

[5] J. Thomas, J. Welde, G. Loianno, K. Daniilidis, and V. Kumar, "Autonomous flight for detection, localization, and tracking of moving targets with a small quadrotor," *IEEE Robot. Autom. Lett.*, vol. 2, no. 3, pp. 1762–1769, Jul. 2017.

[6] D. Wu, D. Chatzigeorgiou, K. Youcef-Toumi, and R. Ben-Mansour, "Node localization in robotic sensor networks for pipeline inspection," *IEEE Trans. Ind. Inform.*, vol. 12, no. 2, pp. 809–819, Apr. 2016.

[7] S. Bartoletti, A. Conti, and M. Z. Win, "Device-free counting via wideband signals," *IEEE J. Sel. Areas Commun.*, vol. 35, no. 5, pp. 1163–1174, May 2017.

[8] R. Estrada, R. Mizouni, H. Otrok, A. Ouali, and J. Bentahar, "A crowdsensing framework for allocation of time-constrained and location-based tasks," *IEEE Trans. Serv. Comput.*, vol. 13, no. 5, pp. 769–785, Sep./Oct. 2020.

[9] F. Zabini and A. Conti, "Inhomogeneous poisson sampling of finite-energy signals with uncertainties in $\mathbb{R}^d$," *IEEE Trans. Signal Process.*, vol. 64, no. 18, pp. 4679–4694, Sep. 2016.

[10] K. Lin, M. Chen, J. Deng, M. M. Hassan, and G. Fortino, "Enhanced fingerprinting and trajectory prediction for IoT localization in smart buildings," *IEEE Trans. Autom. Sci. Eng.*, vol. 13, no. 3, pp. 1294–1307, Jul. 2016.

[11] D. Dardari, A. Conti, C. Buratti, and R. Verdone, "Mathematical evaluation of environmental monitoring estimation error through energy-efficient wireless sensor networks," *IEEE Trans. Mobile Comput.*, vol. 6, no. 7, pp. 790–802, Jul. 2007.

[12] V. Moreno, M. A. Zamora, and A. F. Skarmeta, "A low-cost indoor localization system for energy sustainability in smart buildings," *IEEE Sensors J.*, vol. 16, no. 9, pp. 3246–3262, May 2016.

[13] M. Chiani, A. Giorgetti, and E. Paolini, "Sensor radar for object tracking," *Proc. IEEE*, vol. 106, no. 6, pp. 1022–1041, Jun. 2018.

[14] K. Witrisal *et al.*, "High-accuracy localization for assisted living," *IEEE Signal Process. Mag.*, vol. 33, no. 2, pp. 59–70, Mar. 2016.

[15] J. Werb and C. Lanzl, "Designing a positioning system for finding things and people indoors," *IEEE Spectr.*, vol. 35, no. 9, pp. 71–78, Sep. 1998.

[16] M. Z. Win, F. Meyer, Z. Liu, W. Dai, S. Bartoletti, and A. Conti, "Efficient multi-sensor localization for the Internet of Things," *IEEE Signal Process. Mag.*, vol. 35, no. 5, pp. 153–167, Sep. 2018.

[17] S. D'oro, L. Galluccio, G. Morabito, and S. Palazzo, "Exploiting object group localization in the Internet of Things: Performance analysis," *IEEE Trans. Veh. Technol.*, vol. 64, no. 8, pp. 3645–3656, Aug. 2015.

[18] S. G. Nagarajan, P. Zhang, and I. Nevat, "Geo-spatial location estimation for Internet of Things (IoT) networks with one-way time-of-arrival via stochastic censoring," *IEEE Internet Things J.*, vol. 4, no. 1, pp. 205–214, Feb. 2017.

[19] M. Z. Win, Y. Shen, and W. Dai, "A theoretical foundation of network localization and navigation," *Proc. IEEE*, vol. 106, no. 7, pp. 1136–1165, Jul. 2018.

[20] M. Z. Win, W. Dai, Y. Shen, G. Chrisikos, and H. V. Poor, "Network operation strategies for efficient localization and navigation," *Proc. IEEE*, vol. 106, no. 7, pp. 1224–1254, Jul. 2018.

[21] J. Palacios, G. Bielsa, P. Casari, and J. Widmer, "Single- and multiple-access point indoor localization for millimeter-wave networks," *IEEE Trans. Wireless Commun.*, vol. 18, no. 3, pp. 1927–1942, Mar. 2019.

[22] D. Wang, M. Fattouche, and F. M. Ghannouchi, "Bounds of mmWave-based ranging and positioning in multipath channels," in *Proc. IEEE Globecom Workshops*, 2017, pp. 1–6.

[23] Y. Shen, W. Dai, and M. Z. Win, "Power optimization for network localization," *IEEE/ACM Trans. Netw.*, vol. 22, no. 4, pp. 1337–1350, Aug. 2014.

[24] A. Conti, S. Mazuelas, S. Bartoletti, W. C. Lindsey, and M. Z. Win, "Soft information for Localization-of-Things," *Proc. IEEE*, vol. 107, no. 11, pp. 2240–2264, Nov. 2019.

[25] A. Guerra, F. Guidi, and D. Dardari, "Single-anchor localization and orientation performance limits using massive arrays: MIMO vs. beamforming," *IEEE Trans. Wireless Commun.*, vol. 17, no. 8, pp. 5241–5255, Aug. 2018.

[26] D. Dardari, A. Conti, U. J. Ferner, A. Giorgetti, and M. Z. Win, "Ranging with ultrawide bandwidth signals in multipath environments," *Proc. IEEE*, vol. 97, no. 2, pp. 404–426, Feb. 2009.

[27] S. Bartoletti, W. Dai, A. Conti, and M. Z. Win, "A mathematical model for wideband ranging," *IEEE J. Sel. Topics Signal Process.*, vol. 9, no. 2, pp. 216–228, Mar. 2015.

[28] Z. Abu-Shaban, X. Zhou, T. Abhayapala, G. Seco-Granados, and H. Wymeersch, "Error bounds for uplink and downlink 3D localization in 5G millimeter wave systems," *IEEE Trans. Wireless Commun.*, vol. 17, no. 8, pp. 4939–4954, Aug. 2018.

[29] A. Conti, M. Guerra, D. Dardari, N. Decarli, and M. Z. Win, "Network experimentation for cooperative localization," *IEEE J. Sel. Areas Commun.*, vol. 30, no. 2, pp. 467–475, Feb. 2012.

[30] B. Teague, Z. Liu, F. Meyer, A. Conti, and M. Z. Win, "Network localization and navigation with scalable inference and efficient operation," *IEEE Trans. Mobile Comput.*, to be published, doi: 10.1109/TMC.2020.3035511.

[31] J. C. Aviles and A. Kouki, "Position-aided mm-Wave beam training under NLOS conditions," *IEEE Access*, vol. 4, pp. 8703–8714, Nov. 2016.

[32] Y. Shen and M. Z. Win, "On the accuracy of localization systems using wideband antenna arrays," *IEEE Trans. Commun.*, vol. 58, no. 1, pp. 270–280, Jan. 2010.

[33] P. Addesso, S. Marano, and V. Matta, "Estimation of target location via likelihood approximation in sensor networks," *IEEE Trans. Signal Process.*, vol. 58, no. 3, pp. 1358–1368, Mar. 2010.

[34] G. Papa, P. Braca, S. Horn, S. Marano, V. Matta, and P. Willett, "Multisensor adaptive Bayesian tracking under time-varying target detection probability," *IEEE Trans. Aerosp. Electron. Syst.*, vol. 52, no. 5, pp. 2193–2209, Oct. 2016.

[35] L. Zheng, M. Lops, Y. C. Eldar, and X. Wang, "Radar and communication coexistence: An overview: A review of recent methods," *IEEE Signal Process. Mag.*, vol. 36, no. 5, pp. 85–99, Sep. 2019.

[36] L. Zheng, M. Lops, X. Wang, and E. Grossi, "Joint design of overlaid communication systems and pulsed radars," *IEEE Trans. Signal Process.*, vol. 66, no. 1, pp. 139–154, Jan. 2018.

[37] J. Qian, M. Lops, L. Zheng, X. Wang, and Z. He, "Joint system design for coexistence of MIMO radar and MIMO communication," *IEEE Trans. Signal Process.*, vol. 66, no. 13, pp. 3504–3519, Jul. 2018.

[38] B. Li, A. P. Petropulu, and W. Trappe, "Optimum co-design for spectrum sharing between matrix completion based MIMO radars and a MIMO communication system," *IEEE Trans. Signal Process.*, vol. 64, no. 17, pp. 4562–4575, Sep. 2016.

[39] F. Liu, C. Masouros, A. P. Petropulu, H. Griffiths, and L. Hanzo, "Joint radar and communication design: Applications, state-of-the-art, and the road ahead," *IEEE Trans. Commun.*, vol. 68, no. 6, pp. 3834–3862, Jun. 2020.

[40] F. Liu, L. Zhou, C. Masouros, A. Li, W. Luo, and A. Petropulu, "Toward dual-functional radar-communication systems: Optimal waveform design," *IEEE Trans. Signal Process.*, vol. 66, no. 16, pp. 4264–4279, Aug. 2018.

[41] F. Liu, C. Masouros, A. Li, H. Sun, and L. Hanzo, "MU-MIMO communications with MIMO radar: From co-existence to joint transmission," *IEEE Trans. Wireless Commun.*, vol. 17, no. 4, pp. 2755–2770, Apr. 2018.

[42] A. R. Chiriyath, B. Paul, and D. W. Bliss, "Radar-communications convergence: Coexistence, cooperation, and co-design," *IEEE Trans. Cogn. Commun. Netw.*, vol. 3, no. 1, pp. 1–12, Mar. 2017.

[43] C. B. Barneto, S. D. Liyanaarachchi, T. Riihonen, L. Anttila, and M. Valkama, "Multibeam design for joint communication and sensing in 5G new radio networks," in *Proc. IEEE Int. Conf. Commun.*, 2020, pp. 1–6.

[44] N. Q. Hieu, D. T. Hoang, N. C. Luong, and D. Niyato, "iRDRC: An intelligent real-time dual-functional radar-communication system for automotive vehicles," *IEEE Wireless Commun. Lett.*, vol. 9, no. 12, pp. 2140–2143, Dec. 2020.

[45] X. Yuan, Z. Feng, W. Ni, Z. Wei, and R. P. Liu, "Waveform optimization for MIMO joint communication and radio sensing systems with imperfect channel feedbacks," in *Proc. IEEE Int. Conf. Commun. Workshop,* 2020, pp. 1–6.

[46] X. Yuan *et al.*, "Spatio-temporal power optimization for MIMO joint communication and radio sensing systems with training overhead," *IEEE Trans. Veh. Technol.*, vol. 70, no. 1, pp. 514–528, Jan. 2021.

[47] S. Bartoletti, A. Conti, A. Giorgetti, and M. Z. Win, "Sensor radar networks for indoor tracking," *IEEE Wireless Commun. Lett.*, vol. 3, no. 2, pp. 157–160, Apr. 2014.

[48] Y. Luo, J. A. Zhang, X. Huang, W. Ni, and J. Pan, "Multibeam optimization for joint communication and radio sensing using analog antenna arrays," *IEEE Trans. Veh. Technol.*, vol. 69, no. 10, pp. 11000–11013, Oct. 2020.

[49] S. Bartoletti, A. Giorgetti, M. Z. Win, and A. Conti, "Blind selection of representative observations for sensor radar networks," *IEEE Trans. Veh. Technol.*, vol. 64, no. 4, pp. 1388–1400, Apr. 2015.

[50] J. A. Zhang, X. Huang, Y. J. Guo, J. Yuan, and R. W. Heath, "Multibeam for joint communication and radar sensing using steerable analog antenna arrays," *IEEE Trans. Veh. Technol.*, vol. 68, no. 1, pp. 671–685, Jan. 2019.

[51] Z. Ni, J. A. Zhang, X. Huang, K. Yang, and J. Yuan, "Uplink sensing in perceptive mobile networks with asynchronous transceivers," *IEEE Trans. Signal Process.*, vol. 69, pp. 1287–1300, Feb. 2021.

[52] M. L. Rahman, J. A. Zhang, X. Huang, Y. J. Guo, and R. W. Heath, "Framework for a perceptive mobile network using joint communication and radar sensing," *IEEE Trans. Aerosp. Electron. Syst.*, vol. 56, no. 3, pp. 1926–1941, Jun. 2020.

[53] M. L. Rahman *et al.*, "Enabling joint communication and radio sensing in mobile networks - a survey," Jun. 2020, *arXiv:2006.07559.*

[54] J. H. Winters, "On the capacity of radio communication systems with diversity in Rayleigh fading environment," *IEEE J. Sel. Areas Commun.*, vol. 5, no. 5, pp. 871–878, Jun. 1987.

[55] J. H. Winters, J. Salz, and R. D. Gitlin, "The impact of antenna diversity on the capacity of wireless communication system," *IEEE Trans. Commun.*, vol. 42, no. 2–4, pp. 1740–1751, Feb.–Apr. 1994.

[56] G. J. Foschini, "Layered space-time architecture for wireless communication in a fading environment when using multi-element antennas," *Bell Labs Tech. J.*, vol. 1, no. 2, pp. 41–59, 1996.

[57] M. Z. Win and J. H. Winters, "Virtual branch analysis of symbol error probability for hybrid selection/maximal-ratio combining in Rayleigh fading," *IEEE Trans. Commun.*, vol. 49, no. 11, pp. 1926–1934, Nov. 2001.

[58] E. Telatar, "Capacity of multi-antenna gaussian channels," *Eur. Trans. Telecommun.*, vol. 10, no. 6, pp. 585–595, Nov./Dec. 1999.

[59] M. Z. Win, N. C. Beaulieu, L. A. Shepp, B. F. Logan, and J. H. Winters, "On the SNR penalty of MPSK with hybrid selection/maximal ratio combining over IID Rayleigh fading channels," *IEEE Trans. Commun.*, vol. 51, no. 6, pp. 1012–1023, Jun. 2003.

[60] D. J. Love, R. W. Heath, and T. Strohmer, "Grassmannian beamforming for multiple-input multiple-output wireless systems," *IEEE Trans. Inf. Theory*, vol. 49, no. 10, pp. 2735–2747, Oct. 2003.

[61] M. Chiani, M. Z. Win, and A. Zanella, "On the capacity of spatially correlated MIMO Rayleigh fading channels," *IEEE Trans. Inf. Theory*, vol. 49, no. 10, pp. 2363–2371, Oct. 2003.

[62] H. Shin, M. Z. Win, J. H. Lee, and M. Chiani, "On the capacity of doubly correlated MIMO channels," *IEEE Trans. Wireless Commun.*, vol. 5, no. 8, pp. 2253–2265, Aug. 2006.

[63] A. Conti, M. Z. Win, and M. Chiani, "Slow adaptive M-QAM with diversity in fast fading and shadowing," *IEEE Trans. Commun.*, vol. 55, no. 5, pp. 895–905, May 2007.

[64] E. Bjornson, L. Sanguinetti, J. Hoydis, and M. Debbah, "Optimal design of energy-efficient multi-user MIMO systems: Is massive MIMO the answer?," *IEEE Trans. Wireless Commun.*, vol. 14, no. 6, pp. 3059–3075, Jun. 2015.

[65] A. Conti, W. M. Gifford, M. Z. Win, and M. Chiani, "Optimized simple bounds for diversity systems," *IEEE Trans. Commun.*, vol. 57, no. 9, pp. 2674–2685, Sep. 2009.

[66] M. Chiani, M. Z. Win, and H. Shin, "MIMO networks: The effects of interference," *IEEE Trans. Inf. Theory*, vol. 56, no. 1, pp. 336–349, Jan. 2010.

[67] S. Jeong, O. Simeone, A. Haimovich, and J. Kang, "Beamforming design for joint localization and data transmission in distributed antenna system," *IEEE Trans. Veh. Technol.*, vol. 64, no. 1, pp. 62–76, Jan. 2015.

[68] S. Jeong, O. Simeone, and J. Kang, "Optimization of massive full-dimensional MIMO for positioning and communication," *IEEE Trans. Wireless Commun.*, vol. 17, no. 9, pp. 6205–6217, Sep. 2018.

[69] G. Ghatak, R. Koirala, A. De Domenico, B. Denis, D. Dardari, and B. Uguen, "Positioning data-rate trade-off in mmWave small cells and service differentiation for 5G networks," in *Proc. IEEE 87th Veh. Technol. Conf.*, 2018, pp. 1–5.

[70] R. W. Heath, N. Gonzalez-Prelcic, S. Rangan, W. Roh, and A. M. Sayeed, "An overview of signal processing techniques for millimeter wave MIMO systems," *IEEE J. Sel. Topics Signal Process.*, vol. 10, no. 3, pp. 436–453, Apr. 2016.

[71] O. El Ayach, S. Rajagopal, S. Abu-Surra, Z. Pi, and R. W. Heath, "Spatially sparse precoding in millimeter wave MIMO systems," *IEEE Trans. Wireless Commun.*, vol. 13, no. 3, pp. 1499–1513, Mar. 2014.

[72] K. Venugopal, A. Alkhateeb, N. G. Prelcic, and R. W. Heath, "Channel estimation for hybrid architecture-based wideband millimeter wave systems," *IEEE J. Sel. Areas Commun.*, vol. 35, no. 9, pp. 1996–2009, Sep. 2017.

[73] G. Kwon and H. Park, "Limited feedback hybrid beamforming for multi-mode transmission in wideband millimeter wave channel," *IEEE Trans. Wireless Commun.*, vol. 19, no. 6, pp. 4008–4022, Jun. 2020.

[74] G. Kwon and H. Park, "Joint user association and beamforming design for millimeter wave UDN with wireless backhaul," *IEEE J. Sel. Areas Commun.*, vol. 37, no. 12, pp. 2653–2668, Dec. 2019.

[75] M. Alonzo, S. Buzzi, A. Zappone, and C. D'Elia, "Energy-efficient power control in cell-free and user-centric massive MIMO at millimeter wave," *IEEE Trans. Green Commun. Netw.*, vol. 3, no. 3, pp. 651–663, Sep. 2019.

[76] J. Kim, H. Lee, and S. Chong, "Virtual cell beamforming in cooperative networks," *IEEE J. Sel. Areas Commun.*, vol. 32, no. 6, pp. 1126–1138, Jun. 2014.

[77] M. Steinbauer, A. F. Molisch, and E. Bonek, "The double-directional radio channel," *IEEE Antennas Propag. Mag.*, vol. 43, no. 4, pp. 51–63, Aug. 2001.

[78] B. Hassibi and B. M. Hochwald, "How much training is needed in multiple-antenna wireless links?," *IEEE Trans. Inf. Theory*, vol. 49, no. 4, pp. 951–963, Apr. 2003.

[79] H. Q. Ngo, E. G. Larsson, and T. L. Marzetta, "Energy and spectral efficiency of very large multiuser MIMO systems," *IEEE Trans. Commun.*, vol. 61, no. 4, pp. 1436–1449, 2013.

[80] I. Reuven and H. Messer, "A barankin-type lower bound on the estimation error of a hybrid parameter vector," *IEEE Trans. Inf. Theory*, vol. 43, no. 3, pp. 1084–1093, May 1997.

[81] Y. Shen and M. Z. Win, "Fundamental limits of wideband localization - Part I: A general framework," *IEEE Trans. Inf. Theory*, vol. 56, no. 10, pp. 4956–4980, Oct. 2010.

[82] H. L.Van Trees, *Optimum Array Processing. Part IV of Detection, Estimation, and Modulation Theory*. New York, NY, USA: Wiley, 2002.

[83] Q. Zhang, S. Jin, K. Wong, H. Zhu, and M. Matthaiou, "Power scaling of uplink massive MIMO systems with arbitrary-rank channel means," *IEEE J. Sel. Topics Signal Process.*, vol. 8, no. 5, pp. 966–981, Oct. 2014.

[84] H. Yang and T. L. Marzetta, "Performance of conjugate and zero-forcing beamforming in large-scale antenna systems," *IEEE J. Sel. Areas Commun.*, vol. 31, no. 2, pp. 172–179, Feb. 2013.

[85] J. Mo and J. Walrand, "Fair end-to-end window-based congestion control," *IEEE/ACM Trans. Netw.*, vol. 8, no. 5, pp. 556–567, Oct. 2000.

[86] A. Alkhateeb, O. El Ayach, G. Leus, and R. W. Heath, "Channel estimation and hybrid precoding for millimeter wave cellular systems," *IEEE J. Sel. Topics Signal Process.*, vol. 8, no. 5, pp. 831–846, Oct. 2014.

[87] J. P. Gonzalez-Coma, J. Rodriguez-Fernandez, N. Gonzalez-Prelcic, L. Castedo, and R. W. Heath, "Channel estimation and hybrid precoding for frequency selective multiuser mmWave MIMO systems," *IEEE J. Sel. Topics Signal Process.*, vol. 12, no. 2, pp. 353–367, May 2018.

[88] S. Boyd and L. Vandenberghe, *Convex Optimization*. Cambridge, U.K.: Cambridge Univ. Press, 2004.

[89] A. Alkhateeb, G. Leus, and R. W. Heath, "Limited feedback hybrid precoding for multi-user millimeter wave systems," *IEEE Trans. Wireless Commun.*, vol. 14, no. 11, pp. 6481–6494, Nov. 2015.

[90] G. Kwon, N. Kim, and H. Park, "Millimeter wave SDMA with limited feedback: RF-only beamforming can outperform hybrid beamforming," *IEEE Trans. Veh. Technol.*, vol. 68, no. 2, pp. 1534–1548, Feb. 2019.

[91] ITU-R, "Guidelines for evaluation of radio interface technologies for IMT-2020," ITU-R WP 5D, Tech. Rep. M.2412, 2017.

Hyuncheol Park (Senior Member, IEEE) received the B.S. and M.S. degrees in electronics engineering from the Yonsei University, Seoul, Korea, in 1983 and 1985, respectively, and the Ph.D. degree in electrical engineering from the Georgia Institute of Technology, Atlanta, GA. USA, in 1997.

He was a Senior Engineer from 1985 to 1991, and a Principal Engineer from 1997 to 2002 with Samsung Electronics Co., Korea. Since 2002, he has been with the School of Electrical Engineering, Korea Advanced Institute of Science and Technology, Daejeon, South Korea, where he is currently a Professor. His research interests are in the areas of communication theory and machine learning.

Girim Kwon (Member, IEEE) received the B.S. degree (with highest Hons.) in electrical engineering from the University of Seoul, Seoul, South Korea, in 2013, and the M.S. and Ph.D. degrees in electrical engineering from the Korea Advanced Institute of Science and Technology (KAIST), Daejeon, South Korea, in 2014 and 2020, respectively.

He is a Postdoctoral Fellow with the Wireless Information and Network Sciences Laboratory, Massachusetts Institute of Technology (MIT), Cambridge, MA, USA. His research interests include wireless communications, localization and navigation, signal processing, and machine learning.

Dr. Kwon was the recipient of the S-Oil Best Dissertation Award in 2021, the Best Ph.D. Dissertation Award from KAIST in 2020, and the ICT Paper Award from the Electronic Times in 2018. He was the recipient of the Global Ph.D. Fellowship from the Korean government.

Moe Z. Win (Fellow, IEEE) is a Professor at the Massachusetts Institute of Technology (MIT) and the founding director of the Wireless Information and Network Sciences Laboratory. Prior to joining MIT, he was with AT&T Research Laboratories and with NASA Jet Propulsion Laboratory.

His research encompasses fundamental theories, algorithm design, and network experimentation for a broad range of real-world problems. His current research topics include network localization and navigation, network interference exploitation, and quantum information science. He has served the IEEE Communications Society as an elected Member-at-Large on the Board of Governors, as elected Chair of the Radio Communications Committee, and as an IEEE Distinguished Lecturer. Over the last two decades, he held various editorial positions for IEEE journals and organized numerous international conferences. Recently, he has served on the SIAM Diversity Advisory Committee.

Dr. Win is an elected Fellow of the AAAS, the EURASIP, the IEEE, and the IET. He was Honored with two IEEE Technical Field Awards: the IEEE Kiyo Tomiyasu Award (2011) and the IEEE Eric E. Sumner Award (2006, jointly with R. A. Scholtz). His publications, co-authored with students and colleagues, have received several awards. Other recognitions include the IEEE Communications Society Edwin H. Armstrong Achievement Award (2016), the Cristoforo Colombo International Prize for Communications (2013), the Copernicus Fellowship (2011) and the *Laurea Honoris Causa* (2008) from the Universita degli Studi di Ferrara, and the U.S. Presidential Early Career Award for Scientists and Engineers (2004). He is an ISI Highly Cited Researcher.

Andrea Conti (Senior Member, IEEE) is a Professor and founding director of the Wireless Communication and Localization Networks Laboratory with the University of Ferrara, Italy. Prior to joining the University of Ferrara, he was with CNIT and with IEIIT-CNR.

In Summer 2001, he was with the Wireless Systems Research Department, AT&T Research Laboratories. Since 2003, he has been a frequent visitor to the Wireless Information and Network Sciences Laboratory with the Massachusetts Institute of Technology, Cambridge, MA, USA, where he presently holds the Research Affiliate appointment. His research interests invol theory and experimentation of wireless communication and localization systems. His current research topics include network localization and navigation, distributed sensing, adaptive diversity communications, and quantum information science.

Dr. Conti has served as editor of IEEE journals and chaired international conferences. He was elected Chair of the IEEE Communications Society's Radio Communications Technical Committee and is Co-Founder of the IEEE Quantum Communications & Information Technology Emerging Technical Subcommittee. He received the HTE Puskás Tivadar Medal, the IEEE Communications Society's Fred W. Ellersick Prize, and the IEEE Communications Society's Stephen O. Rice Prize in the field of Communications Theory. He is an elected Fellow of the IET and a member of Sigma Xi. He has been selected as an IEEE Distinguished Lecturer.